



TRIBHUVAN UNIVERSITY
INSTITUTE OF ENGINEERING
PULCHOWK CAMPUS

B-08-BAS-2018/23
**NUMERICAL STUDY OF AIR POLLUTANTS DISPERSION IN AN URBAN
STREET CANYON**

BY:

BIBEK PARAJULI (075AER009)

BINAYAK LOHANI (075AER011)

BIRAJ KHADKA (075AER012)

A PROJECT REPORT SUBMITTED TO DEPARTMENT OF MECHANICAL AND
AEROSPACE ENGINEERING IN PARTIAL FULFILLMENT OF THE REQUIREMENT
FOR THE BACHELOR'S DEGREE IN AEROSPACE ENGINEERING

DEPARTMENT OF MECHANICAL AND AEROSPACE ENGINEERING
LALITPUR, NEPAL

March, 2023

COPYRIGHT

The authors have agreed that the library, Department of Mechanical and Aerospace Engineering, Central Campus Pulchowk, Institute of Engineering may make this project report freely available for inspection. Moreover, the author has agreed that permission for extensive copying of this project report for scholarly purposes may be granted by the professor(s) who supervised the work recorded herein or, in their absence, by the Head of the Department wherein the thesis was done. It is understood that the recognition will be given to the author of this project report and to the Department of Mechanical and Aerospace Engineering, Central Campus Pulchowk, Institute of Engineering in any use of the material of this project report. Copying or publication or the other use of this project report for financial gain without the approval of the Department of Mechanical and Aerospace Engineering, Central Campus Pulchowk, Institute of Engineering, and the author's written permission are prohibited.

Request for permission to copy or to make any other use of this project report in whole or in part should be addressed to:

Head
Department of Mechanical and Aerospace Engineering
Central Campus Pulchowk, Institute of Engineering
Lalitpur, Kathmandu
Nepal

TRIBHUVAN UNIVERSITY
INSTITUTE OF ENGINEERING
CENTRAL CAMPUS PULCHOWK
DEPARTMENT OF MECHANICAL AND AEROSPACE
ENGINEERING

The undersigned certify that they have read, and recommended to the Institute of Engineering for acceptance, a project report entitled "Numerical study of air pollutants dispersion in an urban street canyon" submitted by **Bibek Parajuli, Binayak Lohani and Biraj Khadka** in partial fulfillment of the requirements for the degree of Bachelor of Mechanical and Aerospace Engineering.

Supervisor: **Neeraj Adhikari**, Assistant Professor
Department of Mechanical and Aerospace Engineering
Institute of Engineering, Pulchowk Campus

Supervisor: **Arun Bikram Thapa**, Assistant Professor
Department of Mechanical and Aerospace Engineering
Institute of Engineering, Pulchowk Campus

External Examiner: **Siddhartha Paudel**, Lecturer
Everest Engineering College

Head of Department: **Surya Prasad Adhikari**, Associate Professor
Department of Mechanical and Aerospace Engineering
Institute of Engineering, Pulchowk Campus

DATE: July 20, 2023

ABSTRACT

The alarming increase of hazardous pollutants in South Asian cities such as Kathmandu, Delhi, Mumbai, Dhaka, etc risks the life of every individual there. The situation worsens especially, in the winter rising the air quality index to life-risking situations. A proper scientific study and modeling of the pollutants are necessary in order to manage the pollution level properly. A major source in the production of such harmful pollutants is vehicles and industries. A Computational Fluid Dynamics (CFD) approach is proposed to model the pollutants emitted by vehicles using different Reynolds Averaged Navier Stokes (RANS) turbulence models in the street canyon setup. The primary aim of the study is to understand the effect of turbulence on the transport of gaseous pollutants in the street canyon. This is accomplished by developing a turbulent steady-state solver for the passive transport of pollutants. RNG $k - \varepsilon$ model performed best among other turbulence models with mean FB -0.105, NMSE 0.045, FAC2 0.915 and R 0.93 which is validated with the experimental data. An increase in dispersion of pollutants by 51.4% for AR=0.2 and by 42.33% for AR=0.5 was observed in comparison to AR=1. Street canyons with a low aspect ratio of 0.2 effectively assisted the escape of pollutants. Higher aspect ratios result in flow fields that are more constrained and stagnant, which restricts the dispersion of pollutants. Further, the balconied building lowered the concentration of gaseous pollutants in specific regions only and reduced the exchange concentration flux of pollutants with atmospheric air above the street canyon. Higher wind speeds allowed the concentration to disperse more effectively in Baghbazar's street canyon, resulting in lower concentrations of pollutants.

Keywords: *pollutant, turbulence, aspect ratio, CFD*

ACKNOWLEDGEMENT

This project is prepared in partial fulfillment of the requirement for the bachelor's degree in Mechanical and Aerospace Engineering. We want to start by sincerely thanking our project supervisors, Assistant Prof. Neeraj Adhikari and Assistant Prof. Arun Bikram Thapa, for their constant support and priceless encouragement. It would have been a challenging road for us without their wonderful supervision and advice. Similarly, we are grateful to Assistant Prof. Sudip Bhattarai (PhD) for his expert opinions and suggestions. The authors are also grateful for the assistance of the Digital Research Alliance of Canada, which allowed us to conduct high-fidelity CFD simulations by giving access to the CEDAR supercomputer.

We appreciate the Department of Mechanical and Aerospace Engineering at the Institute of Engineering's Pulchowk Campus for giving us the chance to work together on a project that enabled us to apply the knowledge we had learned during the previous three years in a major project for the fourth year and create a major project of our own that significantly increased our knowledge and gave us new teamwork experiences.

We also want to express our gratitude to all of our friends who assisted us with this effort, both directly and indirectly. Last but not least, we want to express our gratitude to our family members, who have continuously served as sources of inspiration for us.

We will be grateful for and consider any criticism or suggestion.

Authors:

Bibek Parajuli

Binayak Lohani

Biraj Khadka

TABLE OF CONTENTS

| | |
|--|-------------|
| TITLE PAGE | i |
| COPYRIGHT | ii |
| LETTER OF APPROVAL | ii |
| ABSTRACT | iii |
| ACKNOWLEDGEMENT | iv |
| TABLE OF CONTENTS | vi |
| LIST OF FIGURES | viii |
| LIST OF TABLES | ix |
| LIST OF ABBREVIATIONS | x |
| 1 INTRODUCTION | 1 |
| 1.1 Background | 1 |
| 1.2 Problem statement | 3 |
| 1.3 Objectives | 3 |
| 1.3.1 Main objective | 3 |
| 1.3.2 Specific objective | 3 |
| 1.4 Limitations | 4 |
| 2 LITERATURE REVIEW | 5 |
| 3 THEORETICAL BACKGROUND | 8 |
| 3.1 Governing Equations | 8 |
| 3.2 Turbulence Models | 9 |
| 3.2.1 $k - \varepsilon$ model | 10 |
| 3.2.2 SST $k - \omega$ model | 11 |
| 4 METHODOLOGY | 12 |
| 4.1 Solver Development | 12 |
| 4.2 Computational Domain and Mesh Generation | 13 |
| 4.3 Initial and Boundary Conditions | 16 |
| 4.3.1 Inflow boundary condition | 16 |

| | | |
|----------|--|-----------|
| 4.3.2 | Numerical boundary condition | 17 |
| 4.4 | Numerical Solvers | 17 |
| 4.5 | SIMPLE Algorithm | 20 |
| 5 | RESULTS AND DISCUSSIONS | 23 |
| 5.1 | Mesh Sensitivity Analysis | 23 |
| 5.2 | Solver Validation | 24 |
| 5.2.1 | Statistical Performance Measures | 29 |
| 5.3 | Parametric Analysis | 30 |
| 5.3.1 | Aspect Ratio (AR) | 31 |
| 5.3.2 | Addition of balcony structure | 34 |
| 5.4 | Case study of Baghbazar, Kathmandu | 37 |
| 6 | CONCLUSIONS AND RECOMMENDATIONS | 43 |
| 6.1 | Conclusions | 43 |
| 6.2 | Recommendations | 44 |
| | REFERENCES | 45 |
| | APPENDIX | 49 |
| A | SOLVER | 49 |
| A.1 | turbScalarTransportSimpleFoam.C | 49 |
| A.2 | UEqn.H | 51 |
| A.3 | pEqn.H | 51 |
| A.4 | CEqn.H | 53 |
| A.5 | createFields.H | 53 |
| B | Simulation Data | 55 |
| C | Cross-sectional contour plots of pressure and velocity | 56 |
| D | Contour plots of concentration data for two design parameters | 57 |
| E | Contours of concentration at $z/H=0.5$ | 58 |
| F | Streamlines around Baghbazar | 59 |

List of Figures

| | | |
|------|--|----|
| 1.1 | Vehicle emissions | 1 |
| 1.2 | Street canyons in Kathmandu | 2 |
| 2.1 | The flow patterns in street canyon [1] | 6 |
| 4.1 | Flowchart Methodology | 12 |
| 4.2 | CODASC database | 14 |
| 4.3 | Computational domain for validation purpose | 14 |
| 4.4 | Mesh configuration of the domain | 15 |
| 4.5 | First cell height | 15 |
| 4.6 | Atmospheric boundary Layer demonstrated from experiment | 17 |
| 5.1 | Residual plot of RNG $k - \epsilon$ model | 23 |
| 5.2 | Mesh sensitivity analysis evaluated for $c+$ at the coordinates $(-0.06,0,0)$ | 24 |
| 5.3 | Contours of normalized concentration at wall-A | 26 |
| 5.4 | Contours of normalized concentration at wall-B | 27 |
| 5.5 | Streamlines around street canyon | 28 |
| 5.6 | Contour of normalized concentration with velocity vector | 28 |
| 5.7 | (a) N-B: No - Balcony, (b) LW-B: Leeward and Windward - Balcony, (c) L-B: Leeward - Balcony, (d) W-B: Windward - Balcony | 31 |
| 5.8 | Left: Streamlines, Right: Velocity vectors for different aspect ratio (AR) | 33 |
| 5.9 | Bar-chart | 34 |
| 5.10 | Left: Streamlines, Right: Velocity vectors for different balconied structure | 35 |
| 5.11 | Bar-chart | 36 |

| | | |
|------|---|----|
| 5.12 | Street canyon of Baghbazar | 37 |
| 5.13 | Mesh configuration of Baghbazar | 38 |
| 5.14 | Wind speed data in knots measured at 10m AGL, Tribhuvan International Airport [2] | 39 |
| 5.15 | Atmospheric boundary layer for different u_{ref} | 39 |
| 5.16 | Bar-chart diagram for Baghbazar case (C_p/C_s vs wind speed in knots(u_{ref})) | 40 |
| 5.17 | Contours of C_p/C_s for different u_{ref} (a) 1 knot (b) 6 knots (c) 15 knots and (d) 22 knots | 41 |
| 5.18 | Streamlines and Contours of C_p/C_s for different u_{ref} (a) 1 knot (b) 6 knots (c) 15 knots and (d) 22 knots | 42 |
| C.1 | Pressure field | 56 |
| C.2 | Velocity field | 56 |
| D.1 | Wall contours of C_p/C_s for varying aspect ratio: 0.2, 0.5 and 1 | 57 |
| D.2 | Wall contours of C_p/C_s for varying balconied structure: N-B, L-B, W-B and LW-B | 57 |
| E.1 | Contours of C_p/C_s at $z/H=0.5$ for different u_{ref} (a) 1 knot (b) 6 knots (c) 15 knots and (d) 22 knots | 58 |
| F.1 | Streamlines around the street canyon of Baghbazar: (a) 1 (b) 6 (c) 15 and (d) 22 knots | 59 |

List of Tables

| | | |
|-----|---|----|
| 4.1 | Initial data of the wind tunnel experiment | 14 |
| 4.2 | Boundary condition for U | 17 |
| 4.3 | Boundary condition for p | 18 |
| 4.4 | Boundary condition for nut | 18 |
| 4.5 | Boundary condition for k | 18 |
| 4.6 | Boundary condition for omega | 18 |
| 4.7 | Boundary condition for epsilon | 19 |
| 4.8 | Boundary condition for C | 19 |
| 4.9 | Numerical Solvers | 19 |
| 5.1 | Mesh Sensitivity Analysis | 24 |
| 5.2 | Statistical Performance for wall-A | 29 |
| 5.3 | Statistical Performance for wall-B | 29 |
| 5.4 | Height Estimation based on storey of the building [3] | 38 |

LIST OF ABBREVIATIONS

| | |
|--------|--|
| AR | Aspect Ratio |
| ACH | Air Exchange Rate |
| AQI | Air Quality Index |
| AGL | Above Ground Level |
| CFD | Computational Fluid Dynamics |
| CFR | Concentration Flux Ratio |
| CODASC | Concentration Data of Street Canyons |
| CR | Concentration Ratio |
| DOF | Degree of Freedom |
| FAC2 | Fraction of predictions within a factor of two of observations |
| FB | Fractional Bias |
| FOAM | Field Operation and Manipulation |
| H | Height of the building |
| LES | Large Eddy Simulation |
| NMSE | Normalised Mean Square Error |
| R | Correlation coefficient |
| RANS | Reynolds Averaged Navier-Stokes Equations |
| SF | Skimming Flow |
| SKE | Standard $k - \varepsilon$ |
| RNG | Re-Normalisation Group $k - \varepsilon$ |
| RKE | Realizable $k - \varepsilon$ |
| SKO | Standard $k - \omega$ |
| SST | Shear Stress Transport |
| SPM | Statistical Performance Measures |
| TKE | Turbulent Kinetic Energy |
| W | Width of the street |

1. INTRODUCTION

1.1. Background

Air pollution is one of the major challenges humankind is facing in the 21st century. Rapid urbanization, industrialization, increasing number of vehicles, etc are some of the problems faced by the major cities which impact the lives of many people due to air pollution. The air quality index (AQI), which measures the concentration of different elements of air pollution is increasing day by day. Poor air quality leads to severe health problems. Respiratory illness in the lungs, cardiovascular disease, stroke, etc are commonly witnessed in patients nowadays. 4.2 million premature human deaths are recorded every year due to outdoor pollution. According to statistics [4], every nine out of ten people worldwide live in a hazardous environment that exceeds WHO's guidelines of air quality.



Figure 1.1: Vehicle emissions

South Asia is one of the major regions of the world facing an increasing amount of air pollution. Delhi (India) and Beijing (China) are mostly listed as one of the most polluted cities in the world. Sandwiched between these countries, Nepal cannot escape the problems of air pollution [5]. A rapidly urbanizing city like Kathmandu is facing some serious issues of air pollution. It has a population density of 20,288 people per km^2 which is increasing yearly [6]. According to the statistics of the Department of Transport Management (DoTM), the registered motorized vehicles in Nepal have reached 3.1 million in 2021/22 of which more than 25% are in operation in Kathmandu valley alone [7]. Hence, one of the most responsible factors for air pollution is the vehicular emissions caused by the growing number of vehicles in the valley [8]. Out of the vehicular emission, diesel vehicle produces a substantial contribution to the pollution in Kathmandu valley. It is also found that most of these vehicles in Kathmandu use poor-quality fuel and are old and poorly maintained which causes a significant increase in transport emissions in recent years [9]. Some other causes of air pollution

include industrial activities, and residential cooking and heating practices. It is the uttermost concern to resolve the growing air pollution in the valley.

Due to rapid and unplanned urbanization, the number of street canyons in the cities has increased. Street canyons are generally long narrow streets where the building is piled up on either side. Since the number of vehicles moving in the urban streets is increasing rapidly, it has risen vehicular pollution in the streets. This pollution gets trapped inside the street which affects the health of pedestrians and the people living in those buildings. The situation gets worse when the flow is 90° to the street which provides the minimal dispersion of pollutants from the street [10].



Figure 1.2: Street canyons in Kathmandu

Relatively tall buildings with busy narrow streets are also increasing causing the formation of deep street canyons ($H/W > 2$). The places in Kathmandu valley like Kirtipur, New Road, Putalisadak, Baghbazar, etc. have large vehicle mobility with congested roads and buildings on either side. Two-lane roads with three or more storeyed houses on the sides are frequently encountered in Kathmandu. Perpendicular wind flow to the street gives rise to the problem being discussed here. The vehicular pollutant dispersion in these streets needs to be studied properly. The usage of degraded or low-quality fuel in vehicles can cause severe impacts on health. And the emissions of these vehicles on street canyons do not escape out easily to the above atmosphere due to recirculating flow zones created by perpendicular wind flows. Pedestrians and other people near the vicinity breathe in such harmful gas that severely causes health issues in the long run.

The use of numerical modeling techniques in air pollution studies has become increasingly popular in recent years. Numerical modeling provides a cost-effective and efficient way to simulate and predict the dispersion of air pollutants in complex urban environments. Furthermore, numerical modeling allows for the evaluation of different mitigation strategies and the assessment of their effectiveness in reducing air pollutant concentrations. Hence,

in order to investigate the flow pattern created by this kind of urban design to mitigate the above-mentioned problem, a CFD approach will be used for the present study.

1.2. Problem statement

The increasing urbanization has led to a rise in air pollution, which is a major concern for public health. The street canyons in urban areas are known to be hotspots of pollutant concentrations due to their unique geometrical configuration. Therefore, there is a need to develop a deeper understanding of the factors influencing pollutant dispersion in street canyons. The involvement of atmospheric urban wind flows around buildings increases the complexity of the flow problem [11].

Modeling of the emissions from sources such as vehicles as explained above requires a suitable model development. The pollutants such as CO_2 , NO_x , etc was assumed as a scalar quantity that was being transported through an air medium. The study will employ numerical modeling techniques to simulate the flow and dispersion of air pollutants in the Baghbazar street canyon. The first step of the study is to validate the numerical model by comparing it with the wind tunnel experiment data. The validated model will be used to investigate the effects of building geometry and wind speed on the pollutant dispersion within the street canyon. Identifying the optimal building configuration for effective dispersion of pollutants in the Baghbazar street canyon tend to solve the problem of pollution in this area.

1.3. Objectives

1.3.1. Main objective

To perform a numerical study of the pollutant dispersion and impact of building configuration on the flow distribution in the street canyon.

1.3.2. Specific objective

1. To validate the best-suited turbulence model which represents the dispersion of the air pollutants accurately in the street canyon using OpenFoam.
2. To optimize the building configuration using two design parameters: aspect ratio and balconied structure, to assist in effective airflow to mitigate the risk of pollution in the street canyons.

3. To understand the flow pattern of the street canyon in Baghbazar, Kathmandu and study the effect of wind speed on the dispersion of pollutants.

1.4. Limitations

Some of the limitations of this project are listed below:

1. Simulation is limited to the steady state solution in the present study due to the requirement of higher computational time for transient simulation; however, transient solutions could predict the flow and dispersion more accurately.
2. Baghbazar model is unable to depict the actual flow case which excludes factors such as the external pollution source, concentration flow rate, vehicles, utility pole, etc due to its computational constraints. The surrounding buildings are also neglected since they create complex flow such as additional recirculation and reattachment which alters pressure and wind speeds in the street canyon.

2. LITERATURE REVIEW

The vortex present in the street canyon was studied which is typically generated due to shear between the adjacent fluid layers [1, 12]. Aspect ratio (AR), which is the ratio of the height of the building(H) to the width of the street(W), plays a significant role in the canyon street flows. It can be broadly classified as follows:

- **Isolated roughness flow**

Isolated roughness flow refers to the regime where the roughness elements on the building facades are sufficiently large and spaced far enough apart that they do not interact with each other. The flow in this regime is characterized by the formation of vortices around the roughness elements, leading to increased turbulence. Hence, there is a higher dispersion of pollutants from these structures. Isolated roughness flow occurs in street canyons with aspect ratios less than 0.3 ($AR < 0.3$).

- **Wake interference flow**

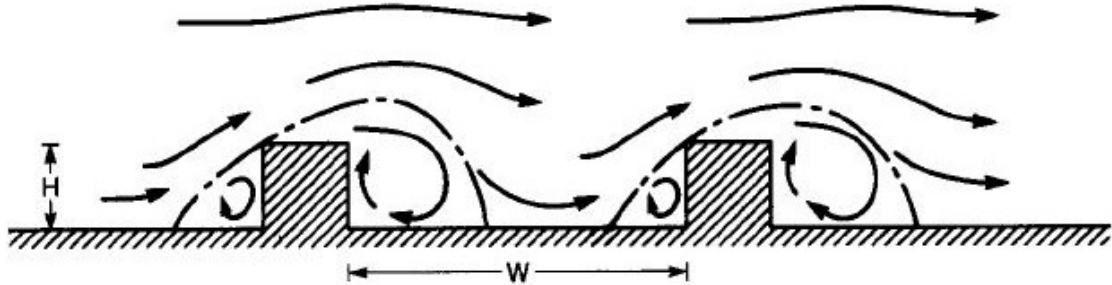
Wake interference flow occurs when the spacing between the buildings is such that the wakes (i.e., the regions of turbulence behind the buildings) interact with each other. This can lead to the formation of large-scale vortices in the canyon, which can have a significant impact on the flow properties. Wake interference flow occurs in street canyons with aspect ratios between 0.3 and 0.7 ($0.3 < AR < 0.7$).

- **Skimming flow regime**

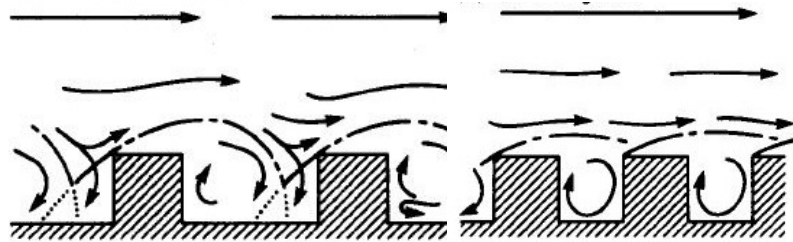
Skimming flow occurs when the buildings are spaced far enough apart that the flow can "skim" over the rooftops of the buildings. In this regime, the flow is relatively uniform and two-dimensional, with little to no turbulence. So the dispersion is relatively low as the flow becomes almost stagnant in the region between the buildings. Skimming flow occurs in street canyons with aspect ratios greater than 0.7 ($AR > 0.7$).

Most of the street canyon configuration resembles the case with $AR > 0.7$ i.e. skimming flow where the pollutants remain trapped inside the canyon. A single recirculation vortex is formed in this type of flow [13]. The primary airflow vortex carries the pollutant emitted by the vehicle to the street canyon's leeward wall, and then upward to the top area of the canyon which allows the air exchange and the escaping of pollutants [14]. The pollutant concentration is therefore greater near the leeward wall than it is near the windward wall [14, 15]. The circulation vortex that is produced in the skimming flow is isolated from the ambient atmospheric flow as shown in Fig. ???. This flow is extensively researched despite

being very ineffective for pollution dispersion for a better understanding to let the pollutants escape out [1].



(a) Isolated roughness flow



(b) Wake interference flow

(c) Skimming flow

Figure 2.1: The flow patterns in street canyon [1]

The wind patterns over the 2D model using SKE turbulent closure scheme for different ARs and wind speeds are studied [16]. Vortices in the canyon increase in number when AR is increased but remain the same after the critical value even if the Reynolds number is increased. A single vortex is formed in the case of skimming flow in the street canyon with $AR \approx 1$. The airflow inside deep street canyons with $AR > 2$ would be significantly more complicated, either with a single vortex or multiple vortices [17, 18, 19, 20]. The Reynolds number normally affected the airflow patterns in deep street canyons [17, 18]. The Reynolds number for the street canyon flows is chosen using the height building and the roof velocity as the reference values[21]. Once the Reynolds number exceeds the critical Reynolds number(Re_c), the flow is not dependent on the Reynolds number[22]. For Reynolds number independence, the sufficient critical Reynolds number for the AR: 1, 1.5, and 2 are 11000, 58000, and 87000 respectively. The critical Reynolds number is a function of the AR of the building [20].

Many of the studies of the canyon street flow are done for the wind direction orthogonal to the street [10, 16]. The flow pattern is changed significantly if the wind direction is changed and found that as the wind direction moves from parallel to perpendicular the average pollutant

amount in the street increases [23]. The 3D effects for the pollutant dispersion in canyon streets are analyzed [24] and the literature discusses the effect of street length on pollutant concentration. Pollutants are able to disperse from the canyon when the flow is dominated by the turbulent process but the mean flow makes the escaped pollutants re-enter the domain [25]. The pollutant will be more diluted in the street canyon when wind speed increases [26].

The presence of balconies in the buildings can significantly impact the flow field and pollutants can escape from the street canyon [27]. The balcony causes less pollutant dispersion and less effective mass exchange of pollutants with the above atmosphere [28]. Street canyon geometry, weather conditions, reactive chemical pollutants, and traffic mobility are the major factors affecting air quality in the urban environment [29]. The real-world street canyons are mostly non-uniform. Generally, two cases arise: step-down and step-up. step-down: the downward building is higher and step-up: the downward building is lower. For the step-down case, the average pollutant concentration is higher and vice versa [30, 31, 32].

Numerous studies have been conducted in the past to predict the dispersion phenomena assisted by turbulent wind using various well-developed turbulence models. SKE and RNG $k - \varepsilon$ models showed similar results for the dispersion in the street canyon setup although both over-predicted the results in comparison to the wind tunnel experiments [33]. RNG $k - \varepsilon$ provides accurate numerical simulation for predicting the pollutant dispersion in a street canyon under various wind speed conditions [34]. A numerical study found that SST $k - \omega$ gave much better results than SKE while completely resolving the viscous sublayer [35]. The $k - \varepsilon$ model with model coefficients; $C_{1\varepsilon} = 1$, $C_{2\varepsilon} = 2.2$, $C_\mu = 0.12$, $\sigma_k = 0.462$ and $\sigma_\varepsilon = 0.42$ provides the improved results against the wind tunnel data [36]. However, in comparison, SKO and SST $k - \omega$ are less investigated than the versions of $k - \varepsilon$ turbulence models. Hence, the present work focuses on the comparison of five different RANS models to develop a clear understanding of the model that closely satisfies the experimental data. Also, steady state RANS may not capture the turbulence phenomena of the concentration of the pollutants perfectly as the flow is complex and of transient nature, [37].

For a CFD study of the urban and environmental flows, blockage ratio and roughness parameters should be defined to fulfill a consistent CFD result [38]. The blockage ratio is the ratio of the frontal area of the building to the frontal area of the computational domain and should not be greater than 3%. Different roughness parameters should be selected based on the inlet, outlet, wall, and other areas of the domain and the appropriate wall function should be determined based on the roughness parameter. The stable and homogeneous line source is necessary for the simulation of vehicular pollution in the urban environment [39]. Turbulent Schmidt numbers highly influence the flow pattern in the pollutant dispersion phenomenon. Sc_t of 0.4 gave the most accurate results for such kinds of flows in the street canyon [40].

3. THEORETICAL BACKGROUND

3.1. Governing Equations

Considering the incompressible effect of the fluids, Navier Stokes equation is discretized using the Finite Volume technique. The combination of mass and momentum equation contributes as NS equation whose mathematical formulation is given as (3.1) and (3.2) respectively.

$$\frac{\partial u_j}{\partial x_j} = 0 \quad (3.1)$$

$$\frac{\partial u_i}{\partial t} + \frac{\partial (u_i u_j)}{\partial x_j} = -\frac{\partial P}{\partial x_i} + \frac{1}{Re} \frac{\partial (\tau_{ij})}{\partial x_j} \quad (3.2)$$

where the notations used by Einstein for the domain's varying x, y, and z directions are I and j = 1, 2, and 3. The instantaneous velocity term in the equation can be visualized as the sum of the fluctuating and mean velocities (3.3).

$$u = u' + \bar{u} \quad (3.3)$$

Now, scalarTransportFoam solver which is generally used for the transport of the passive scalar term has the equation as shown in equation 3.4. This equation is also commonly known as the convection-diffusion equation. The convection-diffusion equation is a fundamental equation in fluid dynamics and is used to describe the transport of a passive scalar in a fluid. It has many applications, including modeling the transport of heat in fluids, the dispersion of pollutants in the environment, and the mixing of chemicals in industrial processes. In the present study, we incorporate this equation to model the pollutant's concentration field.

$$\frac{\partial C}{\partial t} + \frac{\partial (u_i C)}{\partial x_i} = \frac{\partial \left(D_{eff} \frac{\partial C}{\partial x_i} \right)}{\partial x_i} + S \quad (3.4)$$

The first term on the left-hand side represents the time rate of change of the scalar concentration, while the second term represents the convection of the scalar. The convection term depends on the velocity field, u, and the scalar concentration gradient, while the diffusion

term depends on the scalar concentration Laplacian. In the convection-diffusion equation, the convection term represents the advection of the scalar by the fluid, while the diffusion term represents the transport of the scalar due to random molecular motion. Together, these two terms describe the transport of the scalar in the fluid. C represents the scalar parameter or concentration of the pollutant. D_{eff} is the diffusivity term. It represents the sum total of molecular diffusivity (D) and turbulent diffusivity (D_t). Eddy diffusivity is defined as the ratio of eddy viscosity (ν_t) to turbulent Schmidt number (Sc_t). The definition of total diffusivity is given in equation 3.5.

$$D_{eff} = D + \frac{\nu_t}{Sc_t} \quad (3.5)$$

3.2. Turbulence Models

With the mean fluctuating velocity set to zero, RANS equations are time-averaged Navier Stokes equations. The stress tensor responsible for energy loss is known as $\tau_{ij} = -\overline{\rho u_i u_j}$. Turbulence modeling is applied to deal with the closure problem because of τ_{ij} . The most popular RANS turbulence modeling techniques use two-equation models, which use the two parameters turbulence kinetic energy and turbulence length scale. Various models, such as SKE, SKO, SST k - ω , etc., are used to overcome the closure problem that RANS equations produce.

$$k = \frac{3}{2}(u_m I)^2 \quad (3.6)$$

$$\varepsilon = C_\mu \frac{\rho k^2}{\mu} \left(\frac{\mu_t}{\mu} \right)^{-1} \quad (3.7)$$

$$\omega = \frac{\rho k}{\mu} \left(\frac{\mu_t}{\mu} \right)^{-1} \quad (3.8)$$

I = turbulent intensity
 $\left(\frac{\mu_t}{\mu} \right)$ = eddy viscosity ratio.

3.2.1. $k - \varepsilon$ model

In order to mimic the mean flow characteristics under turbulent flow circumstances, the $k - \varepsilon$ model, a two-equation model, is frequently utilized. It is composed of two transport equations (PDEs) that take into consideration the convection and diffusion of turbulence, in addition to conservation equations. The two conveyed variables are turbulent dissipation rate (ε), which describes the rate at which turbulent kinetic energy dissipates, and turbulent kinetic energy (k), which describes the energy in turbulence. It works well for simulating free-shear flows with small pressure gradients, but it might not be appropriate for flows with large pressure gradients and separation. There are various iterations of the $k - \varepsilon$ model, including Standard, Realizable, RNG, etc., all of which are created to function best under particular fluid flow circumstances. The several kinds of $k - \varepsilon$

1. Standard $k - \varepsilon$ model

The k and ε transport equations are

$$\frac{\partial \rho k}{\partial t} + \nabla \cdot (\rho U k) = \nabla \cdot \left[\left(\mu + \frac{\mu_t}{\sigma_k} \right) \nabla k \right] + P_k + P_b - \rho \varepsilon + S_k \quad (3.9)$$

$$\frac{\partial \rho \varepsilon}{\partial t} + \nabla \cdot (\rho U \varepsilon) = \nabla \cdot \left[\left(\mu + \frac{\mu_t}{\sigma_\varepsilon} \right) \nabla \varepsilon \right] + C_1 \frac{\varepsilon (P_k + C_3 P_b)}{k} - C_2 \rho \frac{\varepsilon^2}{k} + S_\varepsilon \quad (3.10)$$

The model coefficients in these equations are: $C_{1\varepsilon} = 1.44$, $C_{2\varepsilon} = 1.92$, $C_\mu = 0.09$, $\sigma_k = 1$ and $\sigma_\varepsilon = 1.3$

2. Realisable $k - \varepsilon$ model

The k and ε transport equations are:

$$\frac{\partial \rho k}{\partial t} + \nabla \cdot (\rho U k) = \nabla \cdot \left[\left(\mu + \frac{\mu_t}{\sigma_k} \right) \nabla k \right] + P_k + P_b - \rho \varepsilon + S_k \quad (3.11)$$

$$\frac{\partial \rho \varepsilon}{\partial t} + \nabla \cdot (\rho U \varepsilon) = \nabla \cdot \left[\left(\mu + \frac{\mu_t}{\sigma_\varepsilon} \right) \nabla \varepsilon \right] + \rho C_1 S_\varepsilon - \rho C_2 \frac{\varepsilon^2}{k + \sqrt{\nu \varepsilon}} + C_{1\varepsilon} \frac{\varepsilon}{k C_{3\varepsilon} P_b + S_\varepsilon} \quad (3.12)$$

The model coefficients in the RKE model are: $C_{1\varepsilon} = 1.44$, $C_2 = 1.9$, $C_\mu = 0.09$, $\sigma_k = 1$ and $\sigma_\varepsilon = 1.2$

3. RNG $k - \varepsilon$ model

Yakhot and colleagues developed the RNG model by utilizing Renormalization Group

techniques to enhance the Navier-Stokes equations. The traditional $k - \varepsilon$ model only takes into account a single turbulence length scale, which results in limited accuracy. The RNG model has an additional term in its ε equation that significantly improves the accuracy for rapidly strained flows. The effect of swirl on turbulence is included in the RNG model, enhancing accuracy for swirling flows. The RNG model, on the other hand, accounts for multiple scales of motion and has shown improved results in modeling rotating cavities. The model coefficients are: $C_{\varepsilon 1} = 1.42$, $C_{\varepsilon 2} = 1.68$, $C_{\mu} = 0.0845$, $\sigma_k = 0.7194$, $\sigma_{\varepsilon} = 0.7194$, $\eta_0 = 4.38$ and $\beta = 0.012$.

4. New-SKE model

This model is exactly similar to the SKE model but has different model coefficients. The model coefficients are: $C_{1\varepsilon} = 1$, $C_{2\varepsilon} = 2.2$, $C_{\mu} = 0.12$, $\sigma_k = 0.462$ and $\sigma_{\varepsilon} = 0.42$ [36].

3.2.2. SST $k - \omega$ model

A popular two-equation model is the SST $k - \omega$ turbulence model, which was created by Menter in 1993. It offers the benefits of both a $k - \omega$ model and a $k - \varepsilon$ model. In the boundary layer, it uses a $k - \omega$ formulation that allows it to be used directly down to the wall, making it useful for low-Re turbulence modeling without any additional damping. In order to avoid becoming overly sensitive to the inlet turbulence qualities, it changes to a $k - \varepsilon$ behavior in the free stream. This model is frequently used because of its success in flows with difficult separation and pressure gradients. It has been seen, though, that locations with high normal strain, including stagnation points and regions with significant acceleration, produce higher turbulence levels. The k and ω transport equations are:

$$\frac{\partial \rho k}{\partial t} + \nabla \cdot (\rho U k) = \nabla \cdot \left[\left(\mu + \frac{\mu_t}{\sigma_k} \right) \nabla k \right] + P_k - \rho \varepsilon \quad (3.13)$$

$$\frac{\partial \rho \omega}{\partial t} + \nabla \cdot (\rho U \omega) = \nabla \cdot \left[\left(\mu + \frac{\mu_t}{\sigma_k} \right) \nabla \omega \right] + \frac{\gamma}{v_t} P_k - \beta \rho \omega^2 + 2(1 - F_1) \frac{\rho \sigma_{\omega 2}}{\omega} \nabla k : \nabla \omega \quad (3.14)$$

4. METHODOLOGY

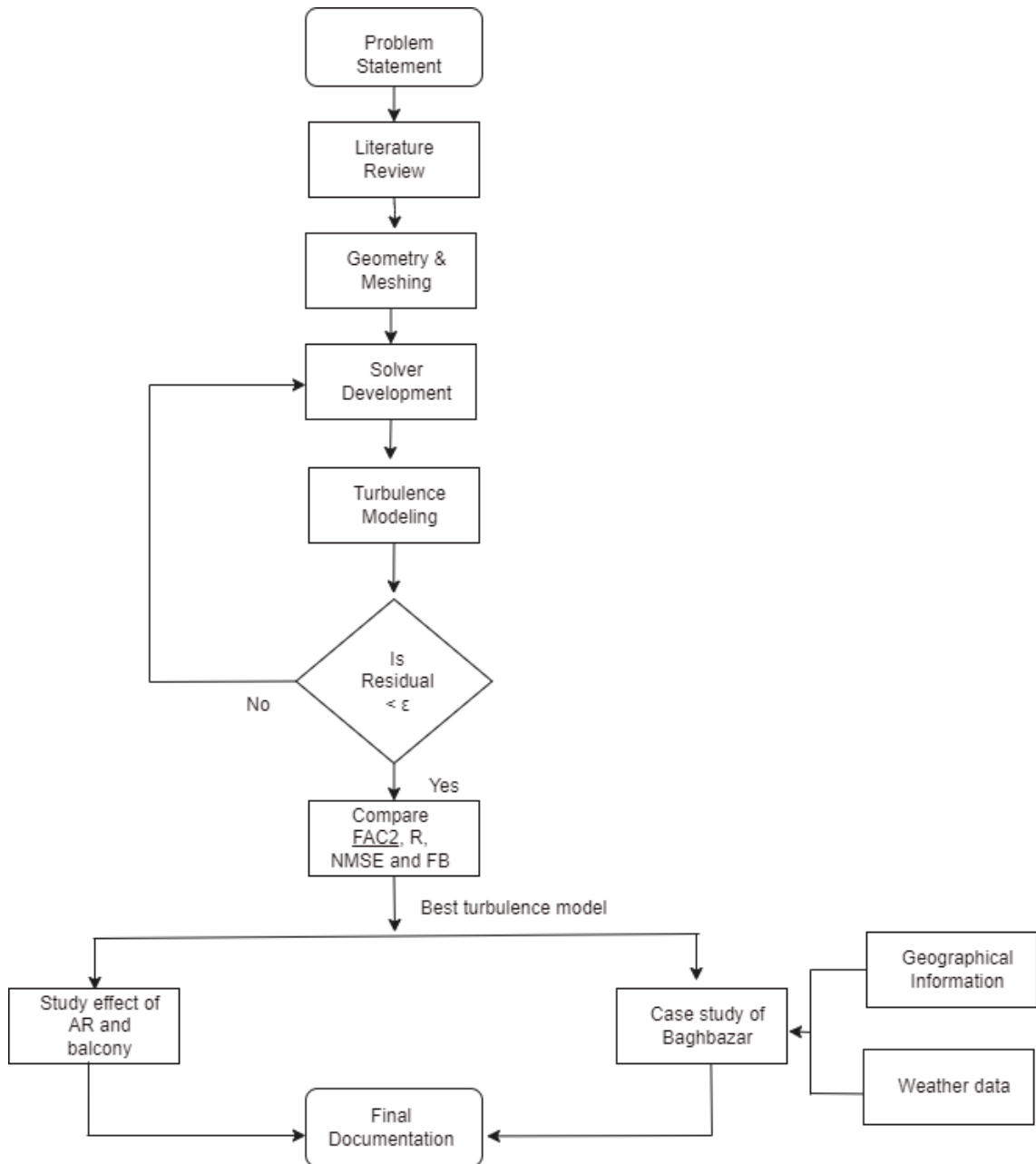


Figure 4.1: Flowchart Methodology

4.1. Solver Development

A combination of simpleFoam and scalarTransportFoam constitutes the development of turb-ScalarTransportSimpleFoam. For the dispersion of the pollutant, a variable C denoting its concentration in ppm is represented in the solver. C acts as a passive scalar that is transported

in a turbulent environment without being actively involved in the physics of the flow. Hence, passive in the sense that the chemical compound comprising the pollutant does not actively react with the ambient air. Equation 3.5 is represented in the OpenFOAM code as shown below:

```

volScalarField DCC ("DCC", D + Turbulence->nut()/Sct) ;

while (simple.correctNonOrthogonal())
{
    fvScalarMatrix CEqn
    (
        fvm::ddt(C)
        + fvm::div(phi, C)
        - fvm::laplacian(DCC, C)
        ==
        fvOptions(C)
    );

    CEqn.relax();
    fvOptions.constrain(KEqn);
    CEqn.solve();
    fvOptions.correct(C);
}

```

4.2. Computational Domain and Mesh Generation

Laboratory of Building- and Environmental Aerodynamics, Karlsruhe Institute of Technology (KIT), Germany has provided the Concentration Data of Street Canyons (CODASC) database for the validation of different street canyon configurations with/without the presence of trees [41]. The model used for the experiment is scaled down by 1:150 as the height of the prototype building and the width of the street is 18m. Similarly, the length of the street canyon is 180m. The solver developed will be validated with the parameters of $H/W = 1$, the wind direction of 90° against the wind tunnel data of the scaled-down model provided by CODASC [41]. Table 4.1 presents the initial parameters provided by the CODASC database.

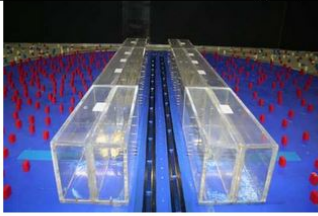
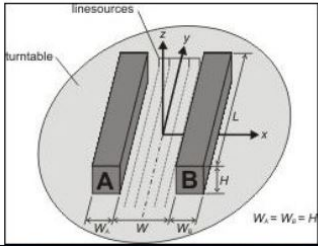
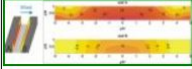
| $W/H = 1$ (aspect ratio: street width W to building height H) | α | TREE PLANTING | normalized concentration data c^+ file name = $[W/H]_{[\alpha]_{[\rho_s]_{[A]_{[wall]}}$ | | concentration contour plot (300 dpi) |
|--|----------|---|---|--|---|
|   | 90° | tree-free (wind perpendicular to street) | 1_90_0,0_000_A.txt 1_90_0,0_000_B.txt | 1_90_0,0_000_A.xls 1_90_0,0_000_B.xls |  1_90_0,0_000.jpg |
| | 45° | tree-free (wind inclined to street) | 1_45_0,0_000_A.txt 1_45_0,0_000_B.txt | 1_45_0,0_000_A.xls 1_45_0,0_000_B.xls | 1_45_0,0_000.jpg |
| | 0° | tree-free (wind parallel to street) | 1_00_0,0_000_A.txt 1_00_0,0_000_B.txt | 1_00_0,0_000_A.xls 1_00_0,0_000_B.xls | 1_00_0,0_000.jpg |

Figure 4.2: CODASC database

Table 4.1: Initial data of the wind tunnel experiment

| Model Parameters | Value |
|-------------------------------------|----------|
| Aspect Ratio (H/W) | 1 |
| Height of the building (H) | 0.12 m |
| Width of the street (W) | 0.12 m |
| Length of the street canyon (L) | 1.2 m |
| Reference velocity (u_{ref}) | 4.65 m/s |
| Reynolds number (Re) | 37,200 |
| Total emission rate from sources | 10g/s |

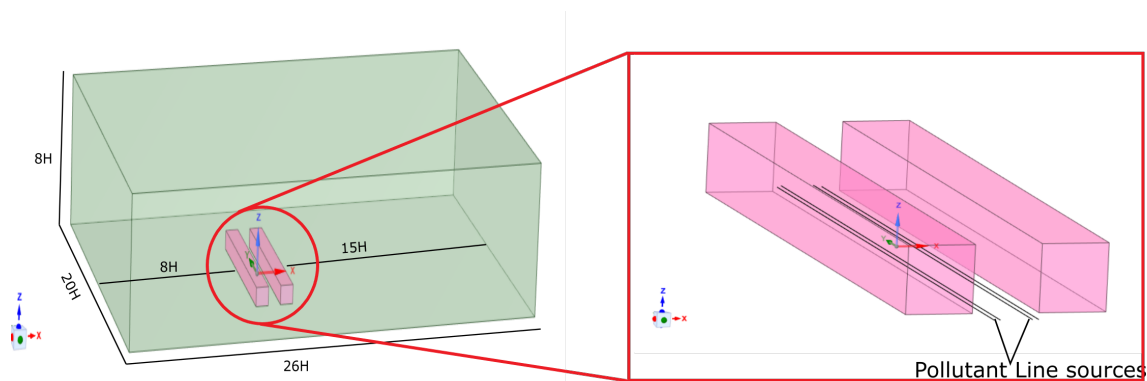


Figure 4.3: Computational domain for validation purpose

The dimension of the geometry is given in table 4.1. Next, the CAD model of the building was imported into the OpenFOAM folder. Further, grid generation was accomplished us-

ing ANSYS Fluent mesher that generates cells in the periphery of the complex watertight geometry from CAD. Mosaic meshing strategy was used in Fluent which is based on the polyhedral meshing approach and is implemented in the Poly-Hexcore mesher. The mosaic meshing approach has several advantages over traditional meshing techniques, including improved accuracy, reduced numerical diffusion, and better capture of flow features. The polyhedral mesh elements used in the technique are better suited for complex geometries such as urban flow environments than traditional tetrahedral or hexahedral elements.

y^+ value of 30 was used at the near walls of the building which lies in the logarithmic boundary layer profile. 189,706 were the hexahedral mesh elements, 27 were prisms and finally, 1,149,049 represented the polyhedral mesh elements constituting 1,338,821 total cells. The maximum skewness of the mesh was 3.17 with a maximum non-orthogonality of 68.21° which ensured the solution will converge.

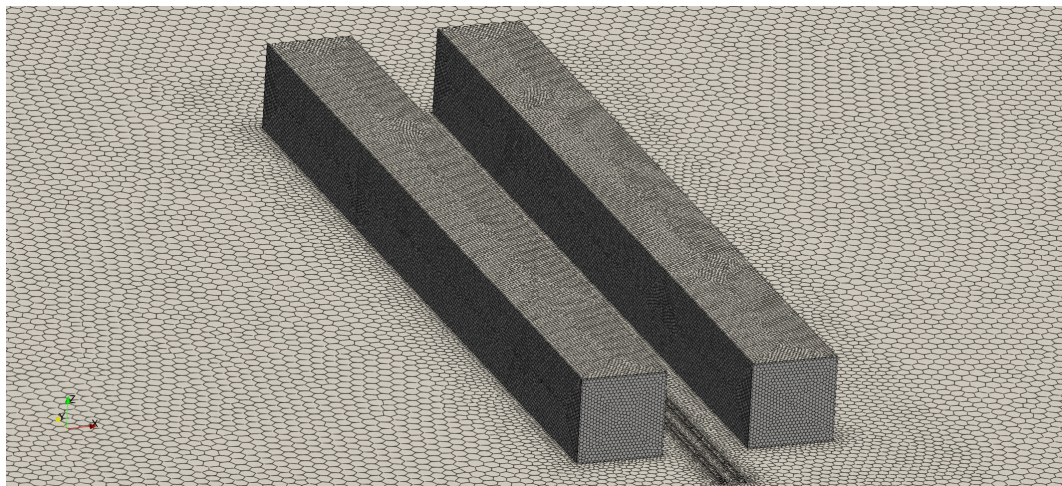


Figure 4.4: Mesh configuration of the domain

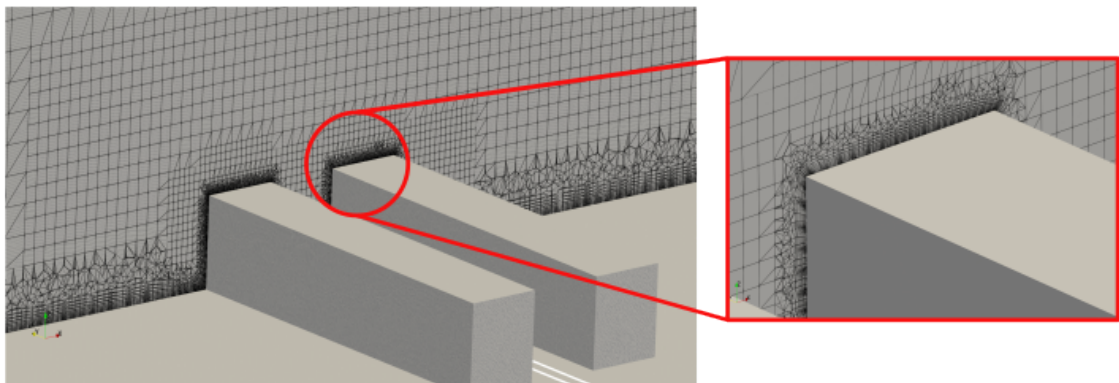


Figure 4.5: First cell height

4.3. Initial and Boundary Conditions

To accurately represent the real-world issue in the case study, a good boundary condition is essential. In the 0 folders, a passive scalar term (C) is added for the pollutant's initialization.

4.3.1. Inflow boundary condition

Depicting a real-world scenario, we require a logarithmic profile of the inlet velocity at the far field known as the atmospheric boundary layer (ABL). ABL is an important concept in urban CFD analysis, particularly in street canyon simulations. The ABL is the layer of air near the earth's surface that is affected by friction with the ground and is influenced by various meteorological factors such as wind speed, temperature, and humidity. In street canyon simulations, the ABL is modeled using appropriate boundary conditions to represent the flow field within and above the canyon. Typically, a velocity profile is specified at the inlet boundary to represent the mean wind speed in the ABL. This profile can be obtained from meteorological measurements or from a meteorological model. The velocity, TKE, and ϵ logarithmic profile are mathematically modeled using the equations in 4.1.

$$U(z) = \frac{u^*}{\kappa} \ln \frac{z+z_0}{z_0}$$

$$\kappa(z) = \frac{u^{*2}}{\sqrt{C_\mu}}$$

$$\epsilon(z) = \frac{u^{*2}}{\kappa(z+z_0)} \quad (4.1)$$

where u^* is the ABL friction velocity, κ is von Karman constant whose value is 0.42, and C_μ a constant with value 0.09. The ABL concept was introduced so that the inlet velocity profile matches the experimental condition conducted at the lab. `atmBoundaryLayerInletVelocity` is an inbuilt boundary condition in OpenFOAM-v2012 that follows the same concept as discussed above. Z_0 , the roughness length as 0.0033; U_{ref} , reference velocity of 4.7 m/s at a given height Z_{ref} of 0.12m are the required parameters defined for this boundary condition. The inlet boundary layer profile is shown in Fig. 4.6.

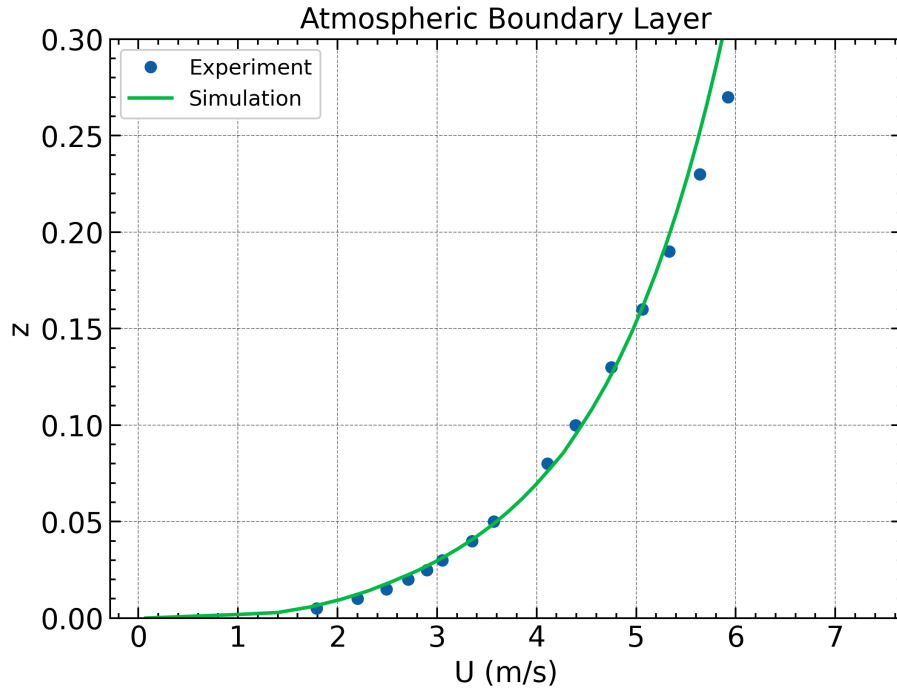


Figure 4.6: Atmospheric boundary Layer demonstrated from experiment

4.3.2. Numerical boundary condition

Furthermore, another boundary condition that requires to be initialized at the beginning is given detailed information in table 4.2-4.8

Table 4.2: Boundary condition for U

| Patch | Condition | Value (ms^{-1}) |
|--------------|-------------------------------|---------------------|
| Inlet | atmBoundaryLayerInletVelocity | (0, 0, 0) |
| Outlet | pressureInletOutletVelocity | (0, 0, 0) |
| ground | noSlip | - |
| building | noSlip | - |
| source | flowRateInletVelocity | 0.01kg/s |
| frontAndBack | symmetry | - |

4.4. Numerical Solvers

For efficient and accurate problem-solving, the Navier Stokes (NS) equation must be discretized using the Finite Volume approach, which necessitates a trustworthy solver. Together with that, another difficult issue for incompressible flows to handle is the pressure-velocity coupling. Therefore, the solvers used for solving the NS equation into the domain of interest

Table 4.3: Boundary condition for p

| Patch | Condition | Value (m^2s^{-2}) |
|--------------|---------------|-----------------------|
| Inlet | zeroGradient | - |
| Outlet | totalPressure | uniform 0 |
| ground | zeroGradient | - |
| building | zeroGradient | - |
| source | zeroGradient | - |
| frontAndBack | symmetry | - |

Table 4.4: Boundary condition for nut

| Patch | Condition | Value (m^2s^{-1}) |
|--------------|-------------------|-----------------------|
| Inlet | calculated | uniform 0 |
| Outlet | calculated | uniform 0 |
| ground | nutkWallFunction | uniform 0 |
| building | nutkWallFunctiont | uniform 0 |
| source | calculated | uniform 0 |
| frontAndBack | symmetry | - |

Table 4.5: Boundary condition for k

| Patch | Condition | Value (m^2s^{-1}) |
|--------------|------------------------|-----------------------|
| Inlet | atmBoundaryLayerInletK | uniform 0 |
| Outlet | inletOutlet | uniform 0.4 |
| ground | kqRWallFunction | - |
| building | kqRWallFunction | - |
| source | fixedValue | uniform 0.4 |
| frontAndBack | symmetry | - |

Table 4.6: Boundary condition for omega

| Patch | Condition | Value |
|--------------|----------------------------|--------------|
| Inlet | atmBoundaryLayerInletOmega | uniform 0 |
| Outlet | inletOutlet | uniform 1.78 |
| ground | omegaWallFunction | - |
| building | omegaWallFunction | - |
| source | fixedValue | uniform 1.78 |
| frontAndBack | symmetry | - |

Table 4.7: Boundary condition for epsilon

| Patch | Condition | Value |
|--------------|------------------------------|---------------|
| Inlet | atmBoundaryLayerInletEpsilon | uniform 0 |
| Outlet | inletOutlet | uniform 0.064 |
| ground | epsilonWallFunction | - |
| building | epsilonWallFunction | - |
| source | fixedValue | uniform 0.064 |
| frontAndBack | symmetry | - |

Table 4.8: Boundary condition for C

| Patch | Condition | Value |
|--------------|--------------|-----------|
| Inlet | fixedValue | uniform 0 |
| Outlet | zeroGradient | - |
| ground | zeroGradient | - |
| building | zeroGradient | - |
| source | fixedValue | uniform 1 |
| frontAndBack | symmetry | - |

are explained in table (4.9). Since a steady state case was solved for the validation of the case study forward-time marching scheme or solver need not be defined. A finite volume method was used for the spatial discretization along with second-order accurate schemes for the discretization of velocity gradient and divergence (Gauss linear scheme).

Table 4.9: Numerical Solvers

| Field | Linear Solver | Smoother | Tolerance |
|-------|----------------|--------------------------|-----------|
| U | Smooth Solvers | Gauss Seidel Smoother | 1e-06 |
| p | GAMG Solver | Gauss Seidel Smoother | 1e-05 |
| nut | Smooth Solvers | Gauss Seidel Smoother | 1e-06 |
| k | Smooth Solvers | Gauss Seidel Smoother | 1e-06 |
| omega | Smooth Solvers | Gauss Seidel Smoother | 1e-06 |
| C | Smooth Solvers | Gauss Seidel Smoother | 1e-06 |

4.5. SIMPLE Algorithm

Since the problem is incompressible and needs to solve the continuity and momentum equations of 1 and 2, it is vital to choose an algorithm that solves these 4 equations and finds a solution for 4 unknowns. The unknown quantities are U_x , U_y , U_z and p . p is the kinematic pressure which is the ratio of static pressure and density of the fluid. The momentum equation is highly non-linear and because there is no specific equation to obtain pressure in an incompressible flow, we propose an iterative algorithm approach to solve the pressure-velocity coupling problem.

$$MU = -\nabla p \quad (4.2)$$

Equation (4.2), gives the linear algebraic form of the momentum equation which is also known as momentum predictor. M is the square matrix with known quantities that are obtained using the Finite-Volume approach in OpenFOAM.

$$AU - H = -\nabla p \quad (4.3)$$

The matrix M is decomposed into diagonal (A) and off-diagonal (H) matrix as in equation (4.3) Now, the velocity equations are solved using the initial conditions and then needs to satisfy the continuity equation.

$$\nabla \cdot (A^{-1} \nabla p) = \nabla \cdot (A^{-1} H) \quad (4.4)$$

Thus, the continuity equation gives an equation for the pressure term which when solved gives the pressure field that can be used to correct the velocity field, so that it satisfies the continuity equation. The corrector loop is repeated until the desired residual is achieved for a single iteration. This process is repeated for different time steps as we are solving transient simulations.

The solver we are using to solve this problem is known as the SIMPLE (Semi-Implicit Method for Pressure Linked Equations) algorithm provided by OpenFOAM.

Step 1: As the velocity field is typically not divergence-free, i.e., it does not fulfill the continuity equation, the momentum equations are calculated from the assumed pressure, p .

Step 2: The pressure equation is solved using obtained velocity field.

Step 3: Divergence-free velocity fields are corrected that is obtained from Step 2. 2 and 3 steps act as corrector loops also called innerCorrectors in OpenFOAM.

Step 4: The turbulence-related fields are then corrected. Those fields are again used to solve the momentum equation in step 1.

Step 5: Loop until desired residual tolerance criteria are met.

```
SIMPLE
{
    residualControl
    {
        p            1e-4;
        U            1e-5;
        "(k|omega|epsilon|C)" 1e-5;
    }
    nNonOrthogonalCorrectors 5;
    pRefCell        0;
    pRefValue       0;
}

relaxationFactors
{
    fields
    {
        p            0.3;
    }
    equations
    {
        U            0.7;
        "(k|omega|epsilon|C).*" 0.7;
    }
}
```

Residual control is used to monitor the convergence of the solution. The residuals represent the difference between the calculated values and the values from the previous iteration and are used as a measure of the accuracy of the solution. Here, the solution is converged when the residual for pressure is below 1E-4 and below 1E-5 for velocity and turbulent parameters fields.

Similarly, non-orthogonal correctors are used in simulations where non-orthogonality exists between the cell faces of a computational mesh. Non-orthogonality refers to the angle between the cell faces not being exactly 90° . Non-orthogonal meshes are common in many real-world simulations and can result in inaccuracies in the results obtained from simulations. To overcome this issue, OpenFOAM provides several non-orthogonal correctors that solve the pressure-velocity coupling problem in non-orthogonal meshes and help to ensure that the simulation results are accurate. In the present study, the maximum non-orthogonality of the mesh was around 68.21° and hence 5 correctors were used in the simulation.

In CFD, relaxation factors are used to accelerate the convergence of the solution. The relaxation factors control the rate at which the pressure, velocity, turbulence parameters and C fields are updated in each iteration. In general, a relaxation factor of 1 means that the variable is updated completely in each iteration, which can result in fast convergence or even instability. A relaxation factor less than 1.0 means that the update is less aggressive, and can help to accelerate convergence. However, too small of a relaxation factor can result in slow convergence. In this simulation, we used a relaxation factor of 0.3 for pressure, 0.7 for velocity and remaining fields.

5. RESULTS AND DISCUSSIONS

The steady-state simulation was performed using the SIMPLE algorithm for the RANS turbulence models. The convergence criteria were specified in terms of residuals which were specified to be 10^{-4} for pressure and 10^{-5} for other fluid flow properties. The convergence in terms of accuracy may not only be represented by infinitesimal residual but also the the flow must be practical in nature. Therefore, to assure the practicality, the volumetric flow rate was checked at the inlets (air and pollutants) and outlet of the domain using post-processing utility and the function object flowRatePatch for summing the net flux on patch faces and came out to be equal to $14.054 \text{ m}^3/\text{s}$ for both considering incompressibility.

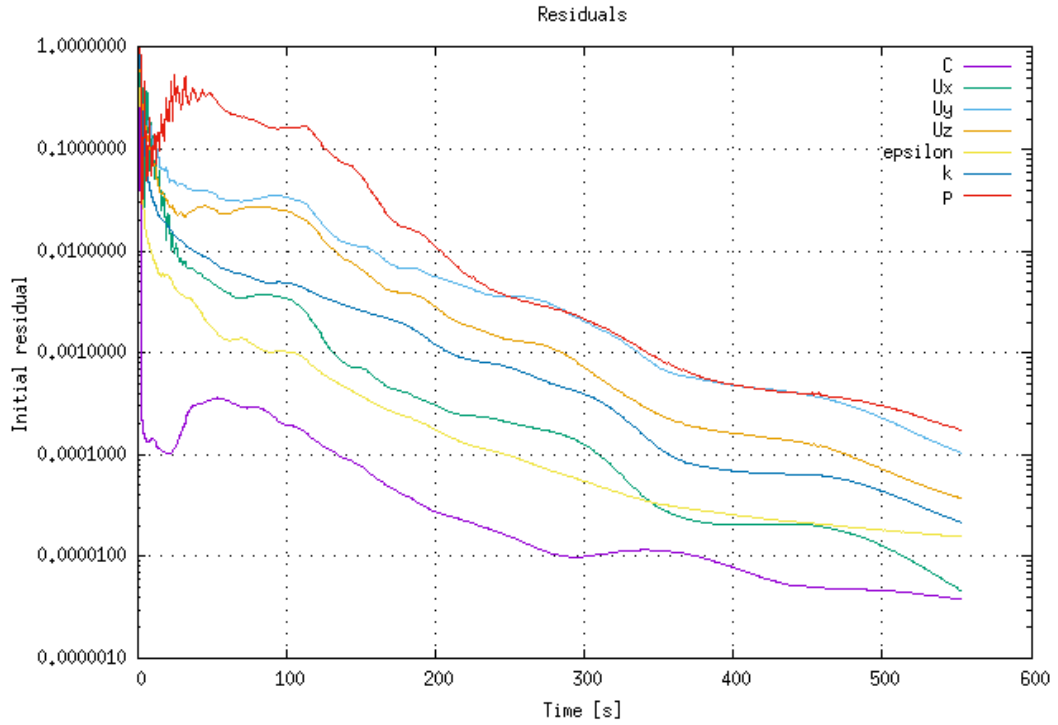


Figure 5.1: Residual plot of RNG $k - \epsilon$ model

5.1. Mesh Sensitivity Analysis

Determining the optimal amount of mesh components is essential to correctly and effectively tackle a particular problem. The outcomes were compared between four distinct mesh configurations that were built. The number of cells produced by ANSYS Fluent mesher is M1, M2, M3, and M4. The maximum concentration (C^+) values at the coordinates $(-0.06,0,0)$ located in wall-A were plotted against various numbers of grids. After thoroughly evaluating

the four mesh options for use, the M3 mesh was ultimately chosen for further analysis. While the M3 and M4 meshes produced similar outcomes, the M4 mesh was larger in size, making it less computationally efficient and potentially less practical for the analysis. Additionally, the M3 mesh was determined to provide a more accurate representation of the flow behavior of the system than the M1 or M2 meshes. As such, the decision to use the M3 mesh was based on a combination of factors including cost efficiency, and practicality.

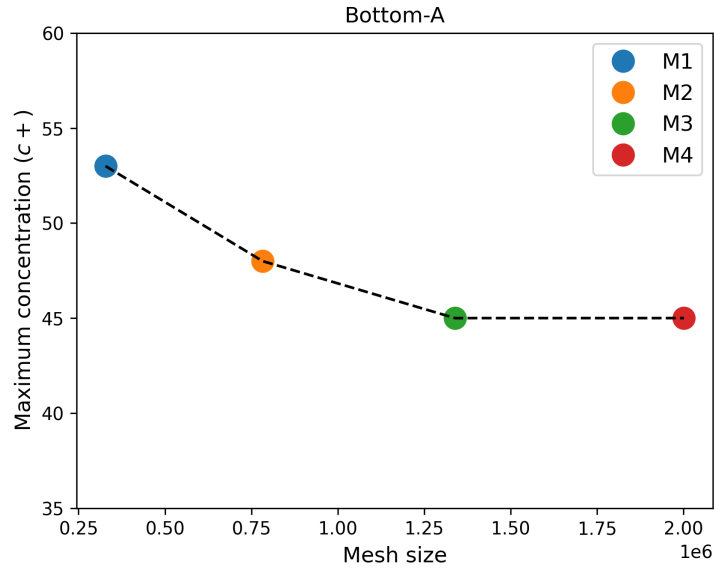


Figure 5.2: Mesh sensitivity analysis evaluated for c^+ at the coordinates $(-0.06,0,0)$

| Mesh configuration | Number of cells |
|--------------------|-----------------|
| M1 | 328,197 |
| M2 | 782,249 |
| M3 | 1,338,821 |
| M4 | 2,001,176 |

Table 5.1: Mesh Sensitivity Analysis

5.2. Solver Validation

As discussed, five RANS simulations: SKE, New-SKE, SST, RKE and RNG are simulated. The converged simulations are compared to the normalized concentration wind tunnel data as shown in equation 5.1. The normalized concentration field (C) was used to define the characteristics of the pollutant in the flow environment given as:

$$C^+ = \frac{C_p U_{ref} H}{C_s Q_s} \quad (5.1)$$

where

C_p =measured concentration in ppm

C_s =source concentration in ppm

U_{ref} =reference velocity at given height

H =Height of the building

Q_s =Source flow rate per unit length in m^2/s

The contours of the normalized concentration field (Figs. 5.3 and 5.4) at the walls of the street canyon are plotted using Paraview and Python. The leeward side of the building is indicated as wall-A and similarly, the windward side is wall-B. Primary vortex is formed between the region between the buildings which is indicated in the streamline plot shown in Fig. 5.5. The presence of this recirculation region is the reason that the gaseous pollutants from the vehicles in the street get trapped there which affects pedestrian health adversely. Turbulence intensity can also play a significant role in the transport of harmful gaseous pollutants and flow behavior is particularly governed by the turbulence induced by building structures. This characteristic behavior is well demonstrated in the vector plot shown in Fig. 5.6; pollutants are circulating in a clockwise manner along with the flow with maximum concentration level at wall-A on the leeward side of the building.

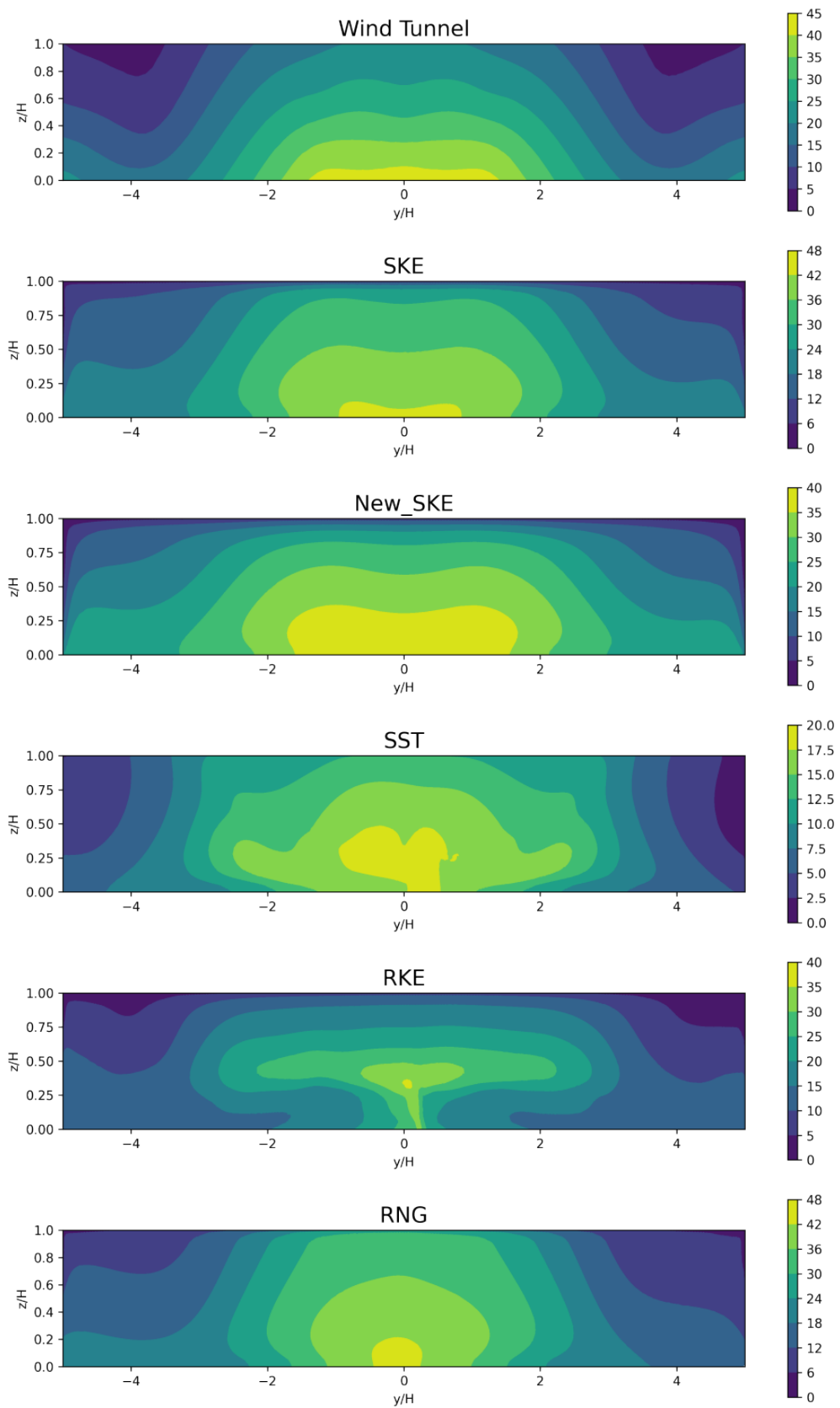


Figure 5.3: Contours of normalized concentration at wall-A

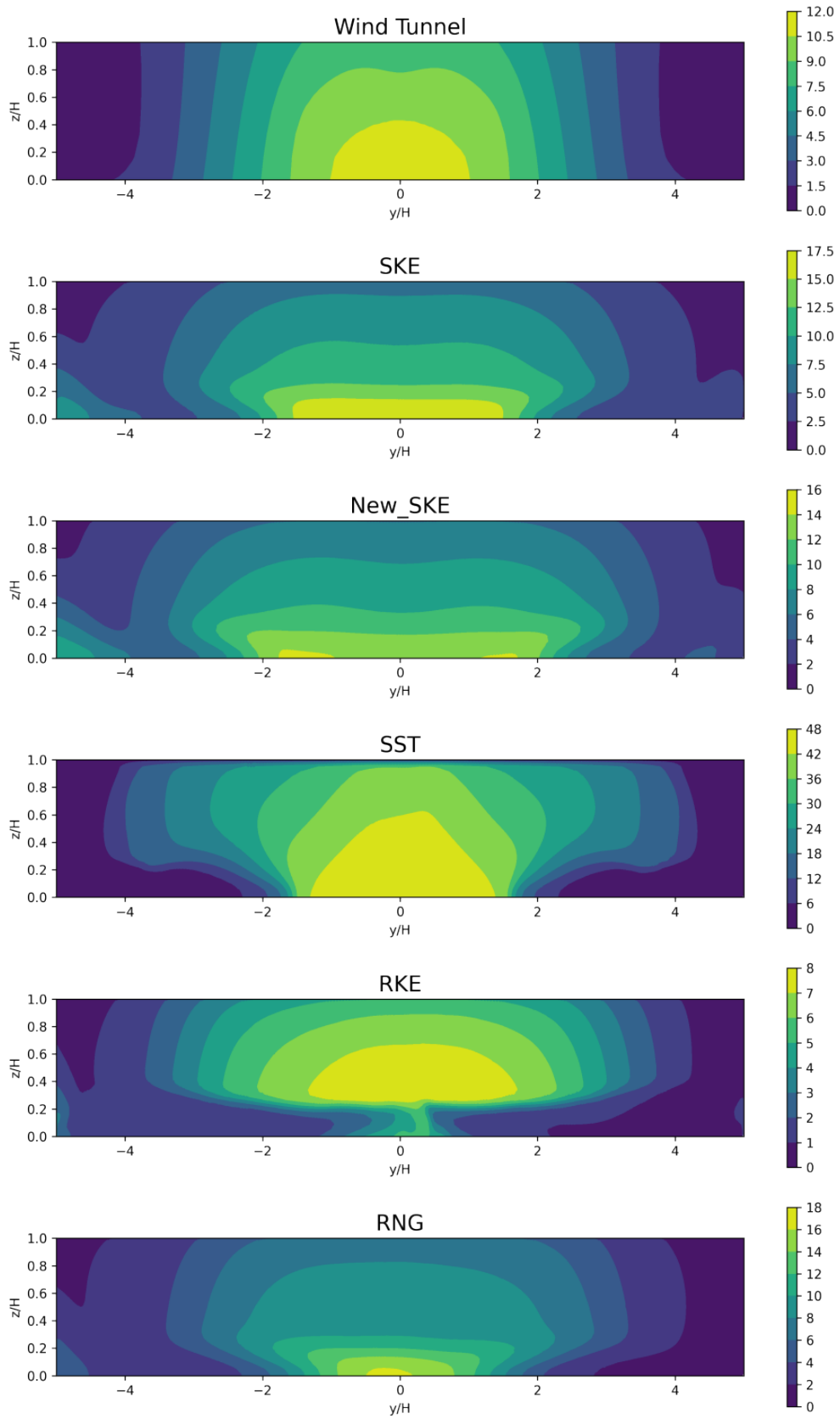


Figure 5.4: Contours of normalized concentration at wall-B

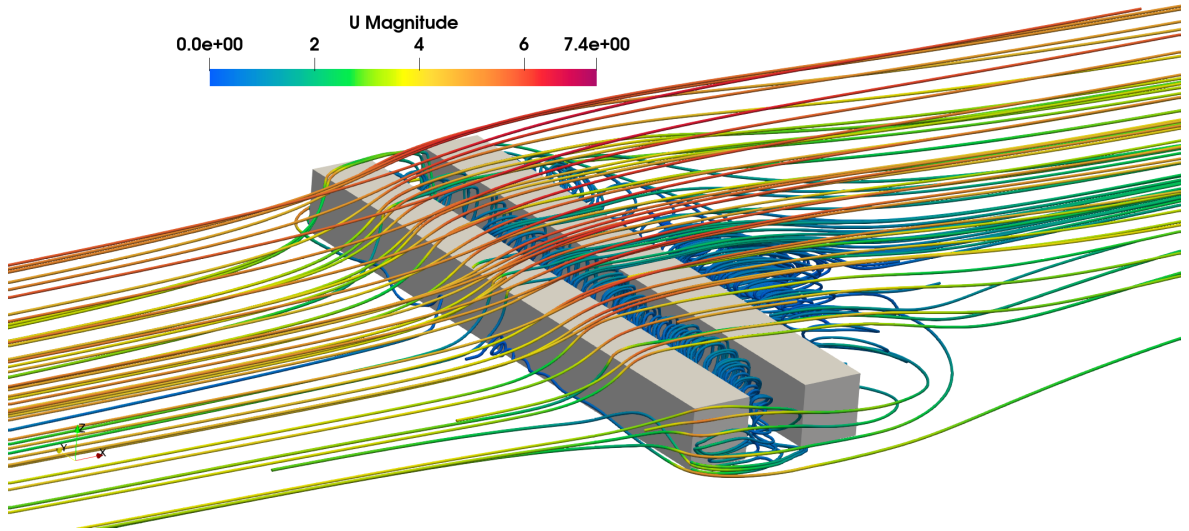


Figure 5.5: Streamlines around street canyon

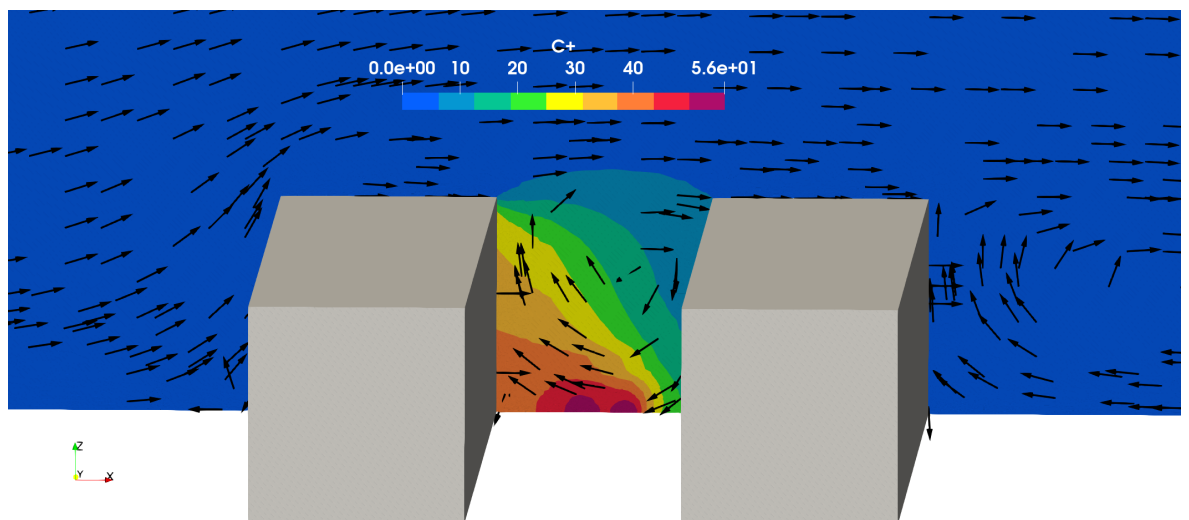


Figure 5.6: Contour of normalized concentration with velocity vector

5.2.1. Statistical Performance Measures

On the basis of four different statistical measures, statistical analysis was carried out. The fractional bias (FB), the normalized mean square error (NMSE), the fraction of predictions within a factor of two of observations (FAC2), and the correlation coefficient (R) were the statistical performance measures (SPM) used for the comparison. RNG- $k - \epsilon$ was chosen in accordance with these SPM.

Table 5.2: Statistical Performance for wall-A

| | SKE | New-SKE | SST | RKE | RNG |
|------|-------|---------|------|------|-------|
| FB | -0.16 | -0.11 | 0.59 | 0.3 | -0.13 |
| NMSE | 0.07 | 0.07 | 0.49 | 0.2 | 0.04 |
| FAC2 | 0.88 | 0.89 | 0.69 | 0.79 | 0.95 |
| R | 0.89 | 0.85 | 0.85 | 0.77 | 0.93 |

Table 5.3: Statistical Performance for wall-B

| | SKE | New-SKE | SST | RKE | RNG |
|------|-------|---------|-------|------|-------|
| FB | -0.28 | -0.25 | -0.13 | 0.45 | -0.08 |
| NMSE | 0.13 | 0.13 | 0.44 | 0.39 | 0.05 |
| FAC2 | 0.74 | 0.67 | 0.29 | 0.78 | 0.88 |
| R | 0.89 | 0.84 | 0.84 | 0.75 | 0.93 |

$$FB = \frac{\overline{C_o} - \overline{C_p}}{0.5(\overline{C_o} + \overline{C_p})} \quad (5.2)$$

$$NMSE = \frac{(\overline{C_o} - \overline{C_p})^2}{\overline{C_o} \overline{C_p}} \quad (5.3)$$

$$R = \frac{(\overline{C_o} - \overline{C_o})(\overline{C_p} - \overline{C_p})}{\sigma_{C_o} \sigma_{C_p}} \quad (5.4)$$

$$FAC2 = \text{fraction that satisfy } 0.5 \leq \frac{C_o}{C_p} \leq 2.0 \quad (5.5)$$

Here, C_o are the wind tunnel measured concentrations.

C_p are predicted by the model.

$\overline{C_o}$ and $\overline{C_p}$ are the mean values of C_o and C_p .
 σ_{C_o} and σ_{C_p} are the SD of C_o and C_p .

A measure of mean bias called FB only reveals systematic errors that result in the simulated values being either overstated or underestimated in relation to the measured values. The numerical difference between C_o and C_p , which is employed as the linear scale's systematic bias, is used. The NMSE is a scatter measure that accounts for both systematic and random errors. R just displays the linear relationship between the measured and predicted values, which is a necessary but insufficient condition for a perfect model because it is sensitive to extreme data pairs. Since it only considers pairs with a ratio between 0.5 and 2.0, FAC2 is the simplest simple metric. This circumstance prevents high and low outliers from having a significant impact on FAC2.

The minimum absolute value for FB and NMSE, and maximum value for FAC2 and R statistical measures signify the best models. Therefore, in all aspects RNG $k - \epsilon$ model gave the best results among others.

5.3. Parametric Analysis

To investigate the impact of design parameters on pollutant dispersion, we conducted a parametric analysis using computational fluid dynamics (CFD) simulations. RNG $k - \epsilon$ model was used to perform this simulation to see the concentration field in the flow vicinity inside the street canyon to perform these studies. Specifically, we varied two design parameters: the aspect ratio (H/W) of the street canyon and the addition of balconies on the building facades.

To quantify the impact of the design parameters on pollutant dispersion, we used two metrics: the Concentration Flux Ratio (CFR) and the Concentration Ratio (CR). The CFR is defined as the ratio of the pollutant concentration flux at a given location to the source inlet concentration flux. The CR is defined as the ratio of the averaged pollutant concentration at a given location to that of original codasc case. The CFR and CR provide a quantitative measure of the efficacy of different design parameters in mitigating air pollution in urban environments. By analyzing these metrics on the building facades at a suitable location, we can gain insight into the impact of different design strategies on pollutant dispersion patterns in street canyons.

$$CFR = \frac{CF_z}{CF_s} \quad (5.6)$$

where

CF_z =Concentration flux at plane $z/H=1$

CF_s =Concentration flux at source

$$CR = \frac{C_w}{C_c} \quad (5.7)$$

where

C_w =Averaged Concentration at a given wall

C_c =Averaged Concentration of a wall from codasc case

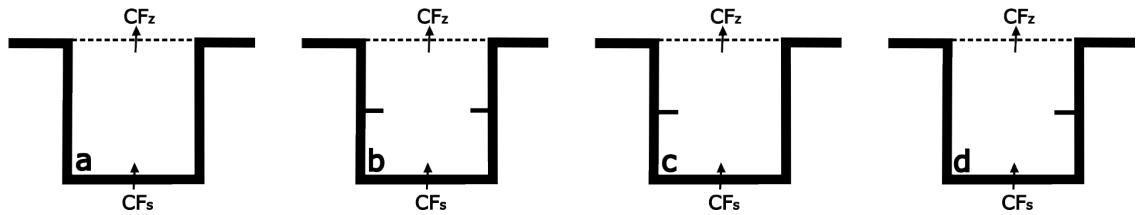


Figure 5.7: (a) N-B: No - Balcony, (b) LW-B: Leeward and Windward - Balcony, (c) L-B: Leeward - Balcony, (d) W-B: Windward - Balcony

5.3.1. Aspect Ratio (AR)

The aspect ratio is one of the most critical parameters for studying pollutant dispersion in street canyon flows. The flow in a street canyon is complex and can be influenced by a variety of factors, including the aspect ratio of the canyon.

At low aspect ratios, the flow in the canyon is primarily dominated by isolated roughness flow, which is characterized by turbulent eddies that develop around obstacles such as buildings and streets. These eddies are relatively small and the resulting flow patterns can promote pollutant dispersion promoting the escape of pollutants from the canyon. As the aspect ratio increases, the flow in the canyon is increasingly influenced by wake interference flow. This type of flow occurs when the wind interacts with the wakes behind buildings, which can create areas of high pressure and low pressure within the canyon. The resulting flow patterns can trap pollutants and prevent them from escaping the canyon, leading to high concentrations of pollutants in the canyon in comparison to the isolated roughness flow. At high aspect

ratios, the flow in the canyon is dominated by skimming flow. This type of flow occurs when the wind flows over the top of the canyon and creates a larger vortex inside the canyon. This assists in the accumulation of pollutants and do not let those pollutants escape the canyon.

Overall, the interaction between these different flow regimes is complex, and the effectiveness of each regime in promoting pollutant dispersion can vary depending on the aspect ratio of the canyon. By understanding the different flow regimes and their interactions, we can design street canyons that are optimized for effective pollutant dispersion and improved air quality. In the study, the three configurations of the increasing aspect ratios are chosen: 0.2 (Isolated roughness flow), 0.5 (Wake interference flow), and 1 (Skimming flow) [1].

1. **AR = 0.2**

The numerical simulations showed that at an aspect ratio of 0.2, the concentration of pollutants in the canyon was relatively low, indicating that the low height of the canyon was promoting effective pollutant dispersion. The streamlines and velocity vectors in Fig. 5.8a of the flow field further supported these findings by showing the formation of vortex structures that allowed for the dispersion of pollutants. These structures were characterized by swirling flow patterns that created two recirculating regions, which helped to draw air and pollutants out of the canyon and into the surrounding environment.

2. **AR = 0.5**

In the numerical study of pollutant dispersion in street canyons, we also analyzed the impact of the aspect ratio of 0.5 on pollutant concentration and dispersion. Results showed that at an aspect ratio of 0.5, the concentration of pollutants in the canyon was higher than at an aspect ratio of 0.2 but lower than at an aspect ratio of 1.

This indicates that while a low aspect ratio of 0.2 may be more effective in promoting the escape of pollutants from street canyons, an aspect ratio of 0.5 can still offer some degree of pollutant dispersion. However, it is important to note that the pollutant concentration at an aspect ratio of 0.5 was still relatively high, highlighting the need for effective urban design strategies to mitigate the impacts of air pollution.

The streamlines and velocity vector plots of the flow field at an aspect ratio of 0.5 in Fig. 5.8b showed the formation of complex flow patterns with elongated vortex structures. These structures were less prominent and less well-defined than those observed at an aspect ratio of 0.2 but still played a role in promoting the escape of pollutants from the canyon.

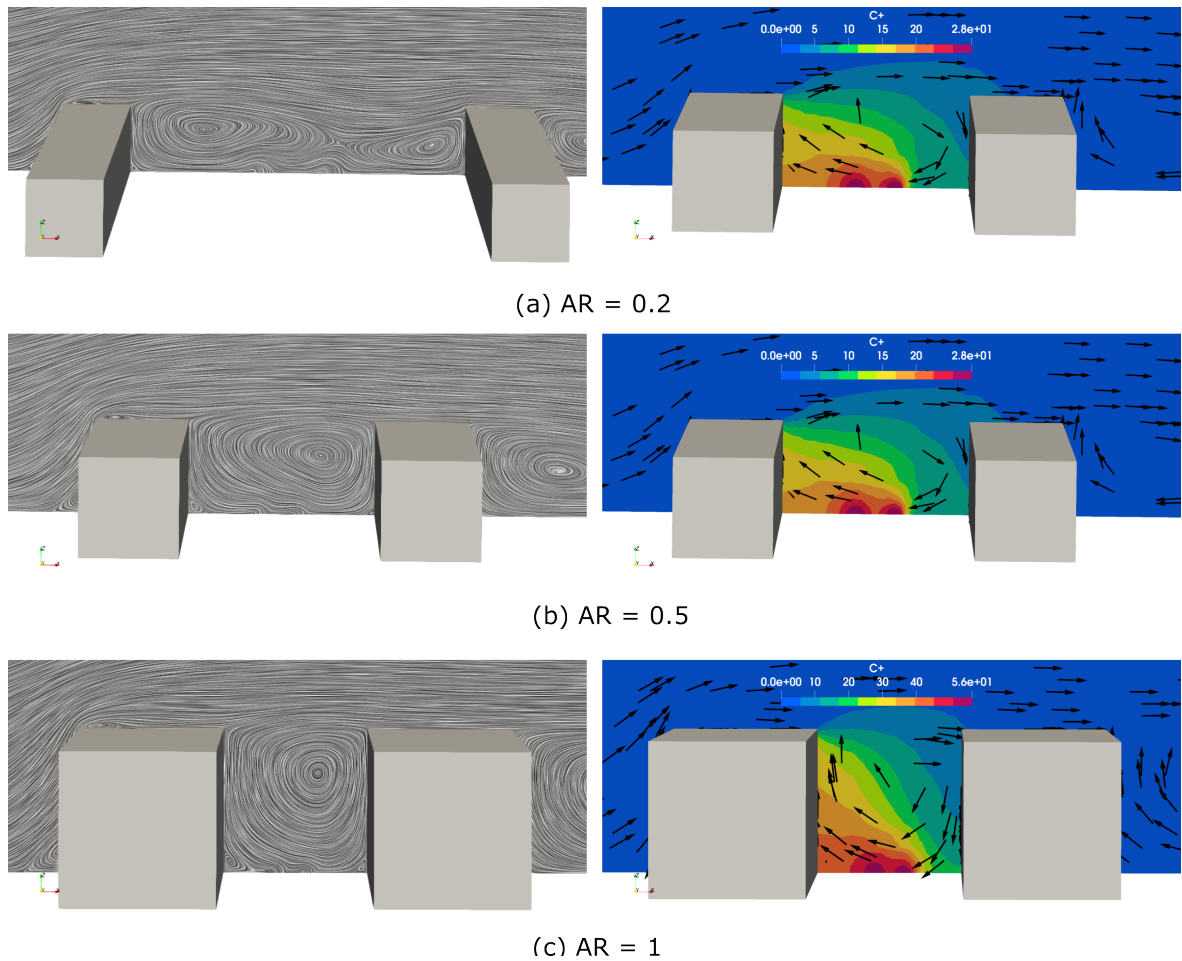


Figure 5.8: Left: Streamlines, Right: Velocity vectors for different aspect ratio (AR)

3. **AR = 1**

The simulations showed that at an aspect ratio of 1 which is the original case of the wind tunnel model used for validation, the concentration of pollutants in the canyon was the highest compared to the aspect ratios of 0.2 and 0.5. This indicates that higher aspect ratios are less effective in promoting the escape of pollutants from street canyons, as the increased height of the canyon walls leads to a more confined and stagnant flow field. The concentration of pollutants at an aspect ratio of 1 was significantly higher compared to the lower aspect ratios, highlighting the need for effective urban design strategies to mitigate the impacts of air pollution in urban environments.

The streamlines and velocity vector plots of the flow field in Fig. 5.8c showed the formation of a large central vortex with a secondary vortex at the corners of the canyon. The flow field was highly confined and stagnant, with little mixing and dispersion of pollutants. This confirms the limitations of higher aspect ratios in promoting pollutant escape and highlights the importance of considering alternative urban design strate-

gies.

Overall, our results indicate that a low aspect ratio of 0.2 can be effective in promoting the escape of pollutants from street canyons. By designing urban environments that incorporate lower aspect ratios and promote the formation of weak vortex structures in the flow field, we can help to reduce the negative impacts of air pollution on public health and the environment.

The bar chart analysis in Fig. 5.9a clearly demonstrated that the aspect ratio of 0.2 resulted in the highest escape of pollutants from the canyon with CFR=1.452, compared to aspect ratios of 0.5 and 1, indicating that this aspect ratio promotes the highest level of pollutant dispersion from the street canyon. On the other hand, the concentration flux ratio decreases as the aspect ratio increases to 0.5 and 1. This is consistent with the observations made in the previous sections, where higher aspect ratios lead to more stagnant and confined flow fields, which limit the mixing and dispersion of pollutants.

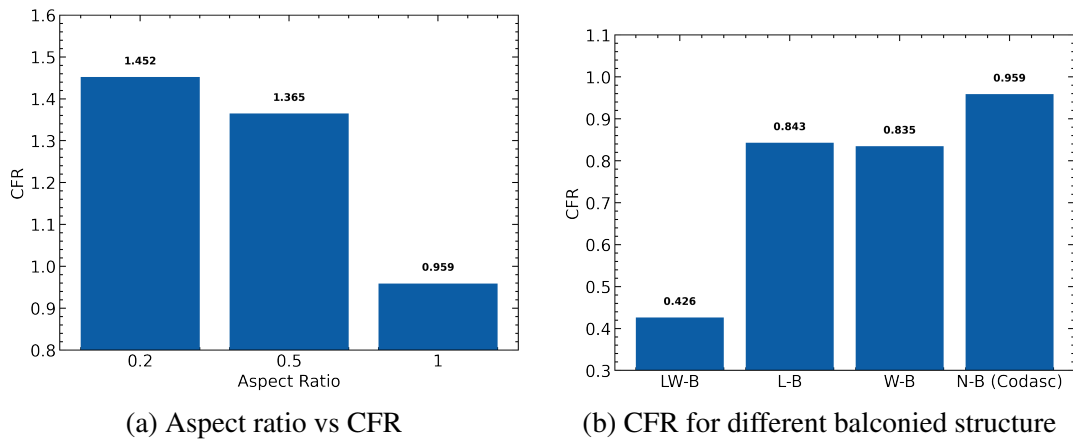


Figure 5.9: Bar-chart

5.3.2. Addition of balcony structure

In addition to the aspect ratio, the addition of balconies can also be an effective design strategy for promoting pollutant dispersion in street canyons. Balconies can create obstructions in the flow field that can lead to the formation of complex flow patterns and vortices, which in turn can affect pollutant dispersion. Specifically, the number and location of balconies on the building faces were varied, while keeping the aspect ratio constant at 1, since this required further study to enhance the dispersion pattern of the pollutants. The impact of adding balconies to the leeward and windward faces of a building, as well as adding balconies to only the leeward or windward face was investigated in the present work.

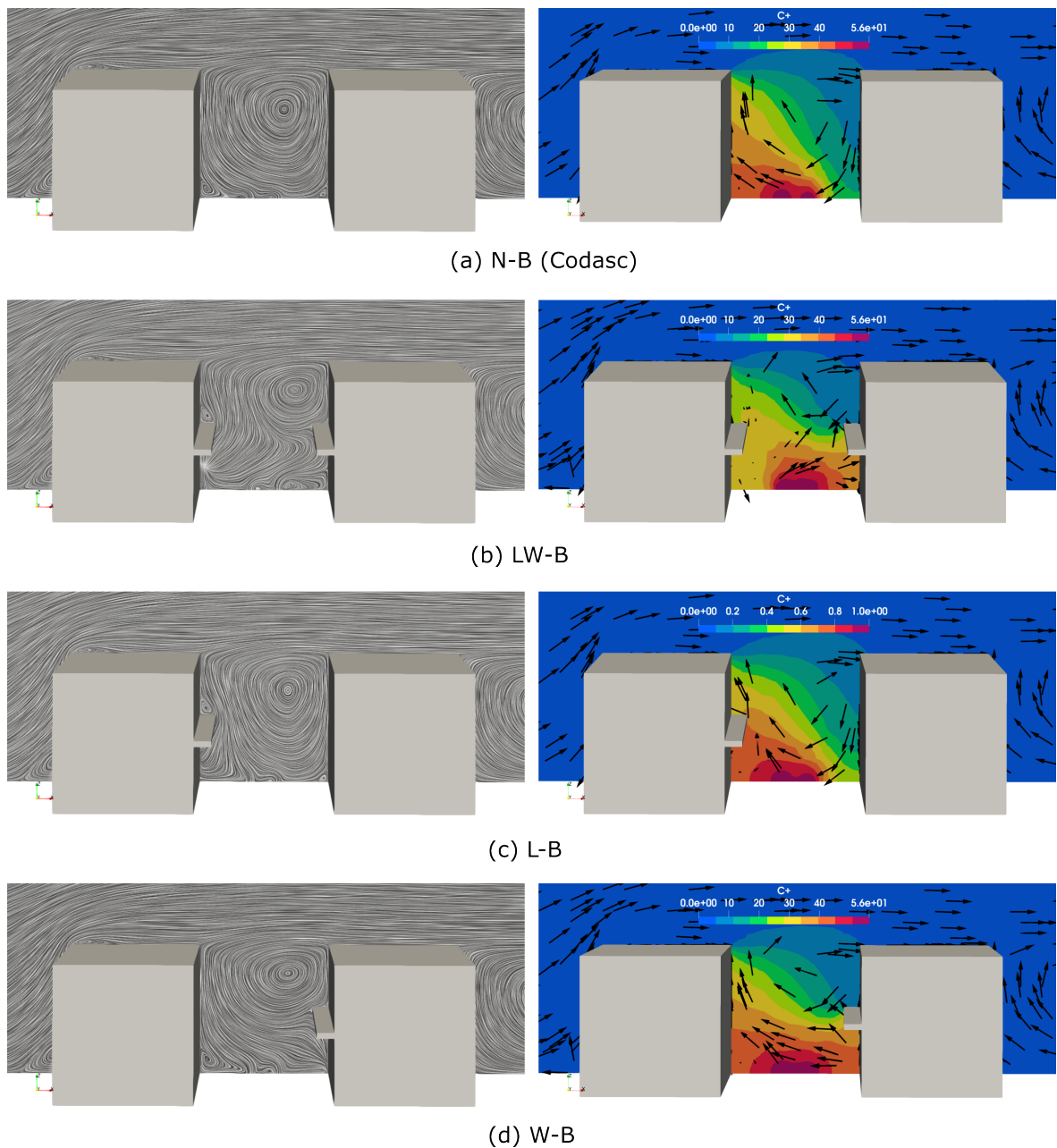


Figure 5.10: Left: Streamlines, Right: Velocity vectors for different balconied structure

1. Two balconies: Leeward and Windward on both wall-A & B

In this study, we added two balconies to both the leeward and windward faces of the building to examine the effect on flow patterns and pollutant dispersion. The addition of balconies on both walls created multiple vortices in the street canyon, as shown in the streamlines 5.10b. It is important to note that while the addition of balconies on both walls created multiple vortices, the resulting flow field was also more stagnant. This is reflected in the concentration flux ratio (CFR) in Fig. 5.9b, which was found to be the least i.e. 0.426 in this configuration compared to others.

The flow pattern generating multiple vortices resulted in the least CFR suggesting that the flow became more stagnant with less dispersion. However, the concentration ratio (CR) at the walls of the top and bottom floors was low on wall-A. This is good for residents in the building or pedestrians on the leeward side, who will experience relatively less pollution. On the other hand, the dispersion of pollutants at the bottom floor on the windward side (wall B) was higher.

2. **Leeward balcony on wall-A** When the balcony was added only to the leeward face of wall-A, the resulting flow pattern was found to be similar to the original codasc's case. The streamlines and velocity vectors showed the development of vortices in agreement with the previously validated model. However, the addition of balconies also led to the formation of a more stagnant flow field, which hindered the escape of pollutants from the street canyon. This is reflected in the CFR value of 0.843, which was found to be the highest among the balconied structures but still less than the case with no balconies.

As noticed in the previous case with LW-B, CR decreased on both floors on the leeward side in comparison to the N-B. On the windward half, the bottom floor concentration is higher by just 11.9% which is far less than the LW-B. Hence, this configuration is better than the LW-B case for pedestrians on the windward side.

3. **Windward balcony on wall-B** When the balcony was added only to the windward face of wall B, the resulting flow pattern was similar to the two-balcony case (LW-B). The flow in the canyon is first obstructed due to the balcony on wall B that breaks down the recirculation region similar to the double balcony case. CFR, in this case, is 0.835 which is slightly less than the L-B case; however, despite the similar flow pattern with LW-B, CFR, in this case, is quite high.

In comparison with the N-B, the dispersion of pollutants on wall-A is almost comparable, however, the concentration on the bottom floor of wall-B is greatly increased by 173.9% so, the health of the pedestrian or residents on this portion is at stake.

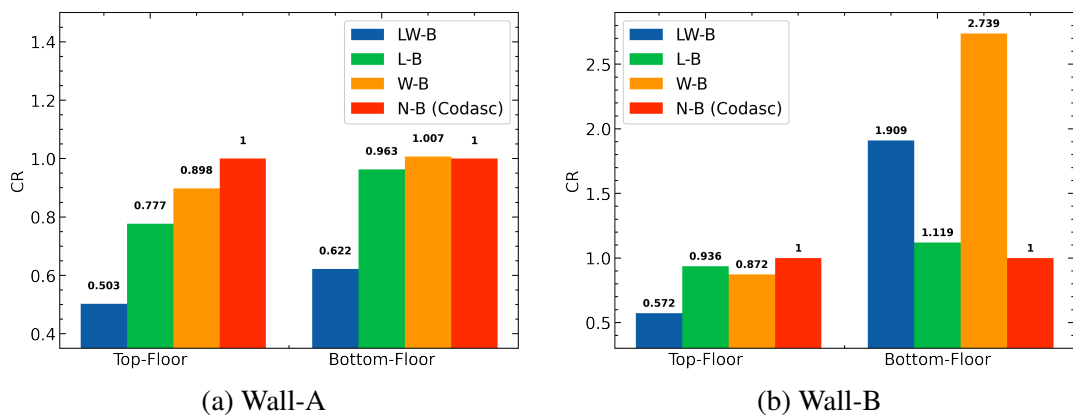


Figure 5.11: Bar-chart

All in all, these results indicate that the addition of balconies can help to reduce the concentration of gaseous pollutants in certain areas (especially on the top and bottom floor of wall A and only the top floor of wall B) but may not be effective in all situations. It is therefore important to carefully consider the design of balconies and their placement in buildings to achieve the desired outcomes.

5.4. Case study of Baghbazar, Kathmandu

The most commonly found street canyon setup in Kathmandu consists of a two-lane street with three to four-storeyed buildings on either side. This results in the formation of a deep street canyon. One of the rising issues of severe air pollution in the urban cities of South Asian countries is the increased number of vehicles. The majority of vehicles in Kathmandu are over 20 years old, and the lack of proper maintenance to emission standards has led to the release of harmful pollutants into the atmosphere. In the street canyons of Kathmandu, where tall buildings are in close proximity to the road, the dispersion of these pollutants is further restricted, leading to increased concentrations and health risks for the local population.

A configuration of a 12m wide street and 116m street length was chosen for the analysis from Baghbazar, Kathmandu as the AQI is quite high in this area (maximum $PM_{2.5} = 200 \mu g/m^3$) [42]. Baghbazar is a densely populated area with high traffic volume, which makes it an ideal location for the study of pollutants emitted from vehicles. A narrow street canyon with high buildings on both sides, which can lead to the formation of complex flow patterns and pollutant dispersion mechanisms qualifies Baghbazar as an ideal place to conduct further study.

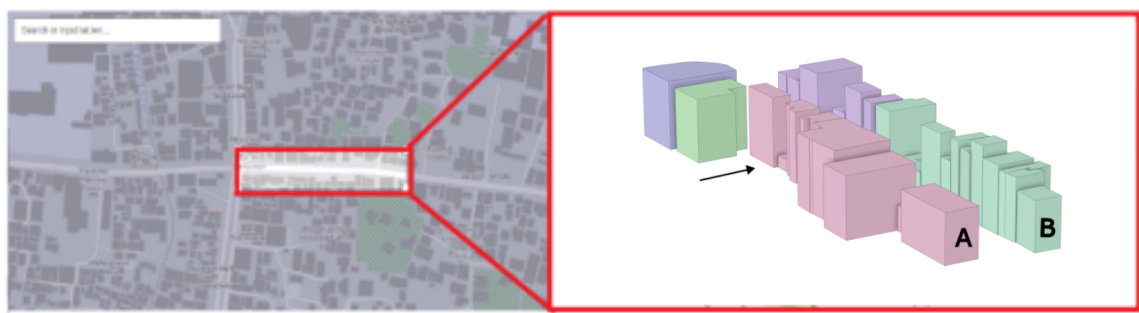


Figure 5.12: Street canyon of Baghbazar

This area comprises 31 buildings altogether which include Medium Rise (6 to 8 Storey) and General buildings (1 to 5 Storey). A two-dimensional sketch of Baghbazar was extracted from Cadmapper [43]. Due to the lack of enough data on the individual height of the build-

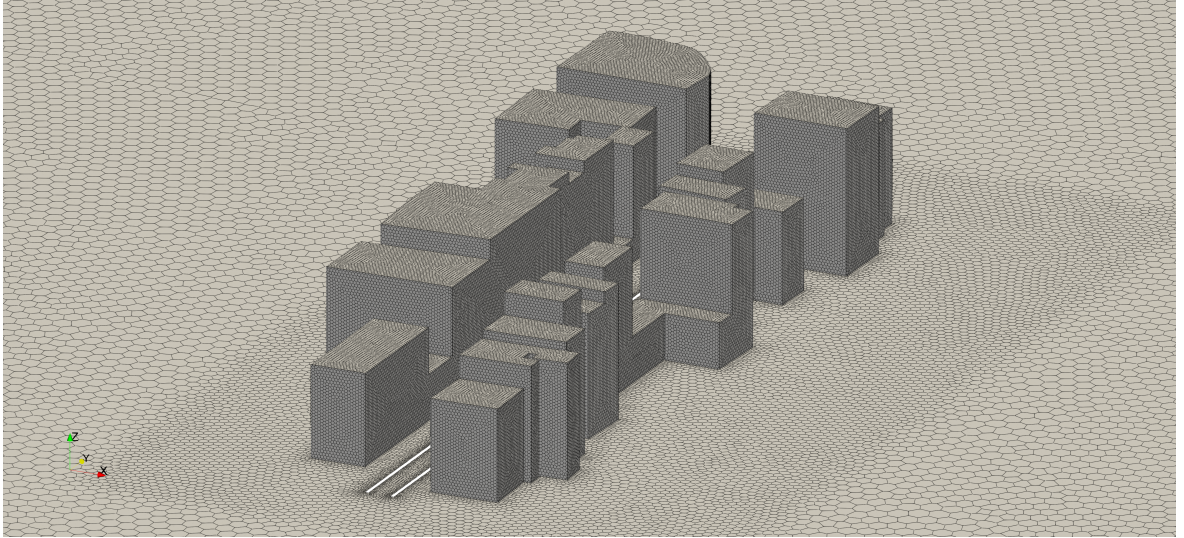


Figure 5.13: Mesh configuration of Baghbazar

ings in this area, a site visit was conducted to note this data. Height is an important parameter to take into consideration for the accurate replication of the flow pattern using the numerical method. Since measuring the exact height of all these buildings was not physically possible due to various reasons, a different strategy was approached where the storey of each of the buildings was noted. After the calculation of the height of the building from table 5.4, data were manually inserted in the ANSYS designer software called SpaceClaim, as shown in Figure F.1. The total emission rate from the source was taken as 1.5kg/s (full-scale) which is similar to that of the base case used previously for validation(N-B). Although this would be an important parameter to consider in the accurate modeling of pollutant dispersion in the vicinity, our primary aim was mainly to understand the dynamics of the flow pattern. Hence, data was not collected in this regard and the former value was chosen for further analysis.

Table 5.4: Height Estimation based on storey of the building [3]

| Type | Storey | Height |
|-------------------|--------|------------|
| General Buildings | 1 to 5 | below 16m |
| Medium Rise | 6 to 8 | 16m to 25m |

Next, an important parameter to consider is the wind speed and its direction. Aligning with the objective of the project, perpendicular speed direction with respect to the street was considered which is responsible to generate the recirculating regions that trap the gaseous pollutants in the canyon. Although other wind directions could drastically affect flow physics, this path is out of scope in the present study. Variation in wind speed is a common phenomenon occurring in the real world. In order to gain insights into the impact of velocity magnitude on the flow behavior and dispersion of pollutants, the study was conducted for 4 different

magnitudes: 1, 6, 15, and 22 knots.

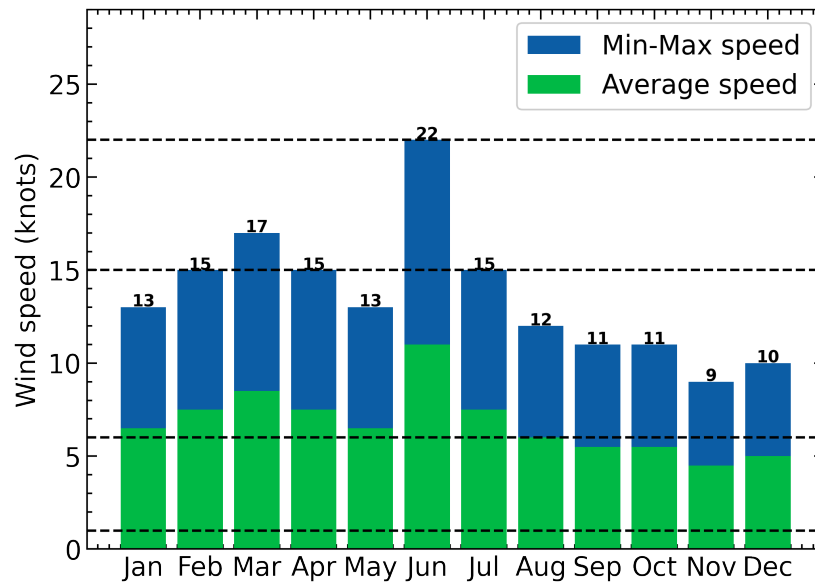


Figure 5.14: Wind speed data in knots measured at 10m AGL, Tribhuvan International Airport [2]

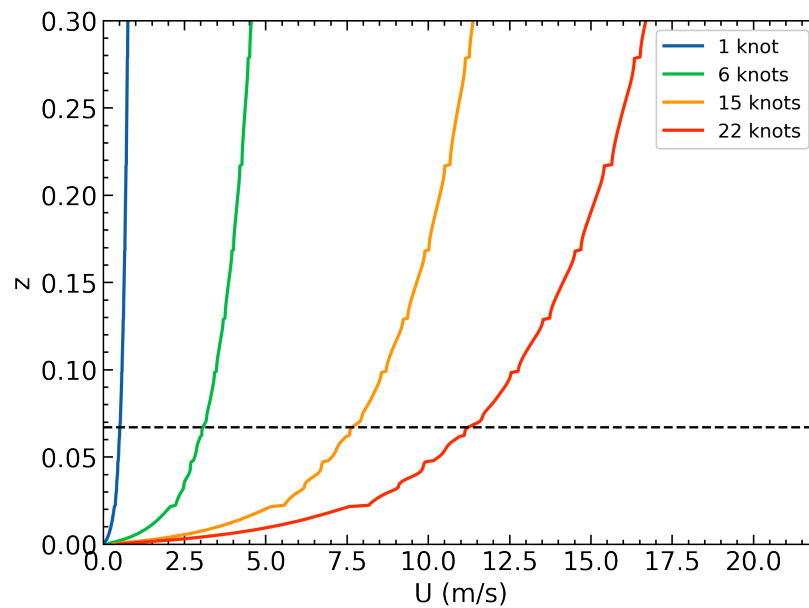


Figure 5.15: Atmospheric boundary layer for different u_{ref}

The atmospheric boundary layer (ABL) was plotted for four different reference velocities for the wind data collected 10m AGL as shown in Fig. 5.15. The plot of ABL shows the relationship between wind speed and height AGL. The average height of the building was 16.28m resulting in the Reynolds numbers 521,680, 3,175,050, 7,735,250 and 11,692,820 respectively. As discussed previously, all these Reynolds numbers surpassed the critical

Reynolds number for the given $H/W=1.35$. Hence, the vortex structures in the scaled-down model are similar to its prototype. With this understanding, the model was scaled down to 1:150 and simulation was performed in OpenFOAM using the RNG turbulence model. The wind velocity is normally 1-22 knots which correspond to a wind scale in the range of 1 to 9.

The C_p/C_s decreases on building A and building B as wind velocity increases, as shown in the bar chart in Fig. 5.16. Wind velocity is an important parameter in pollutant dispersion. The dilution of pollutants in the street canyon increases as wind velocity increases. The increment in wind velocity also aids in improving wind pressure on the building surface, promoting the natural ventilation of buildings in the street canyon[44]. This is also evident in the contour 5.17 where pollutant concentration on both building A and building B has decreased as the wind velocity increases. Looking at the contours in Fig. E.1, the value of C_p/C_s is higher near building A than building B. The wall of building B(windward wall) experiences downflow velocity faster than the level flow near the ground and flow on the wall of building A(leeward wall) causing the formation of a large vortex. This vortex allows the accumulation of pollutants on the leeward wall which results in a higher concentration of pollutants on the leeward wall than on the windward wall. The streamlines shown in Fig. 5.18 is evident that the change in flow velocity greatly affects the flow pattern inside the street canyon. Hence, the dispersion of pollutants from the source is governed by the recirculating airflow.

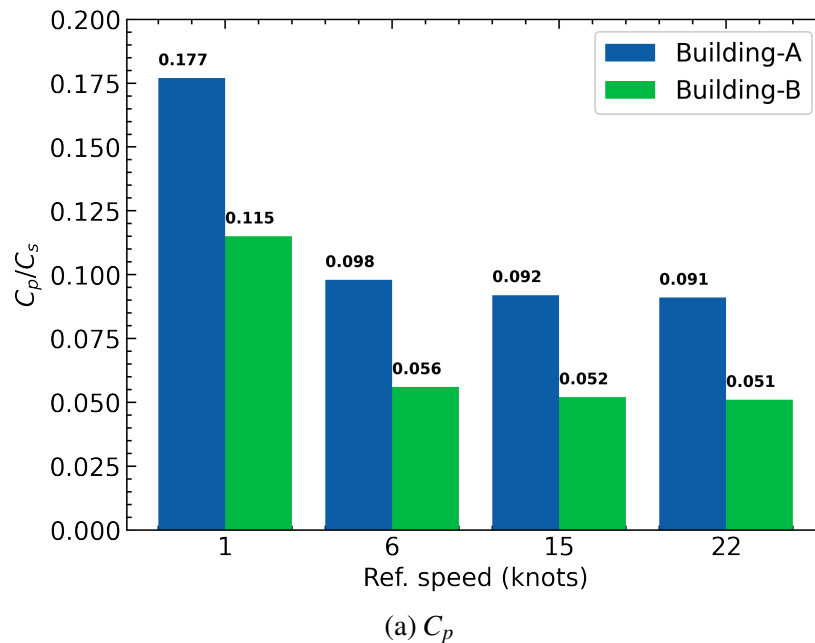


Figure 5.16: Bar-chart diagram for Baghbazar case (C_p/C_s vs wind speed in knots(u_{ref}))

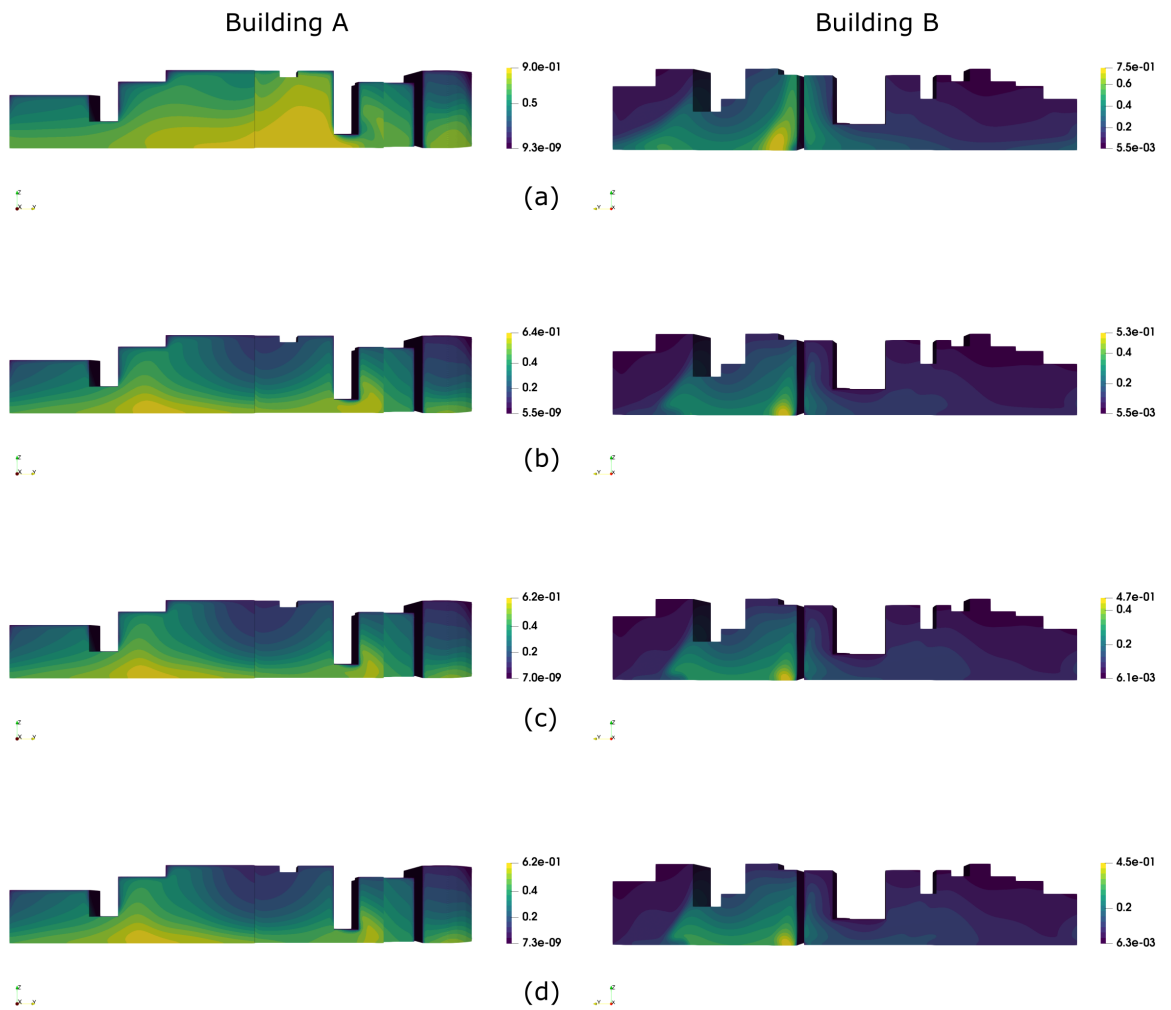


Figure 5.17: Contours of C_p/C_s for different u_{ref} (a) 1 knot (b) 6 knots (c) 15 knots and (d) 22 knots

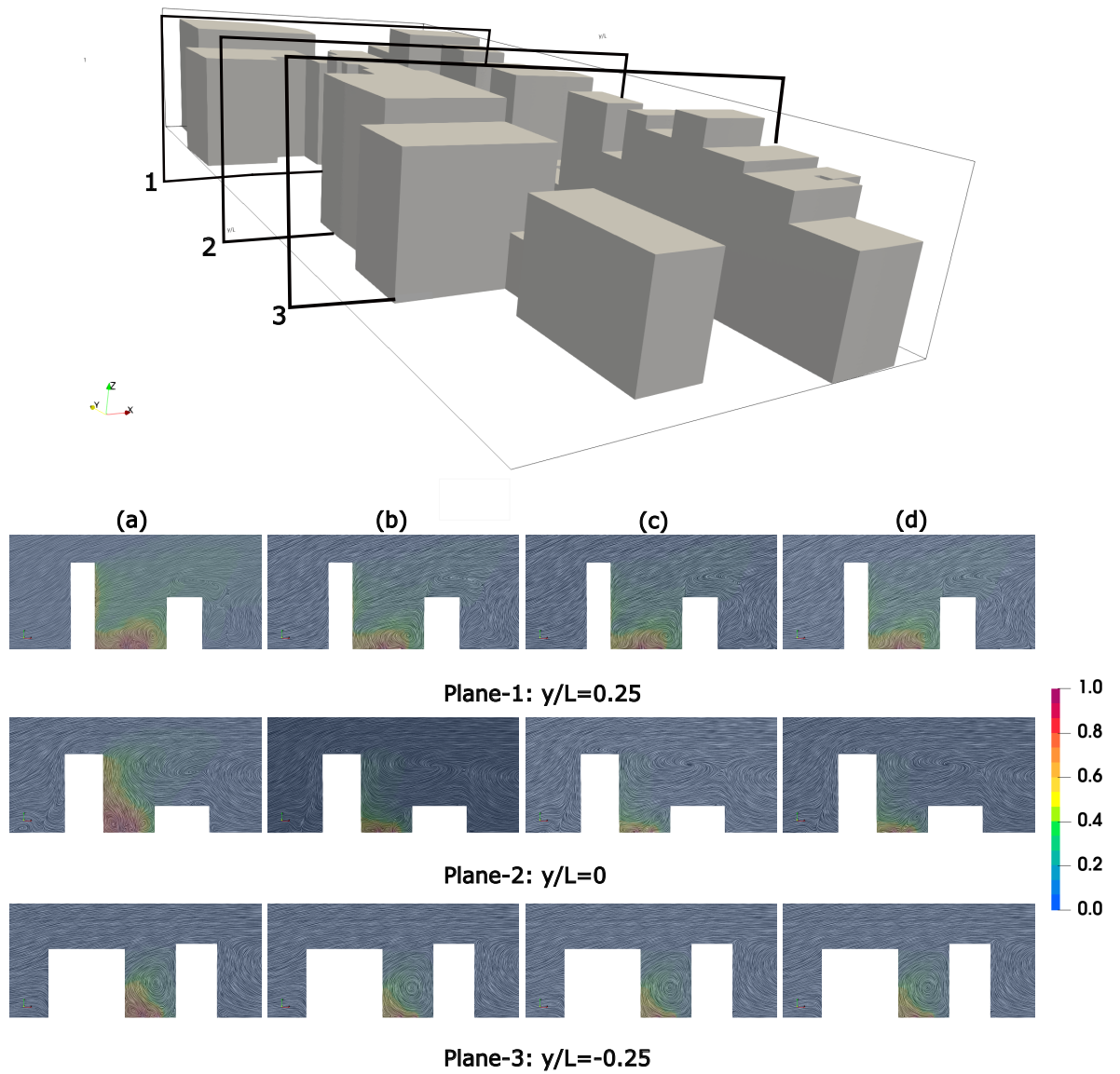


Figure 5.18: Streamlines and Contours of C_p/C_s for different u_{ref} (a) 1 knot (b) 6 knots (c) 15 knots and (d) 22 knots

6. CONCLUSIONS AND RECOMMENDATIONS

6.1. Conclusions

Five distinct RANS turbulence models were used for the computational investigation of pollutants dispersion, and the results were validated using experimental data from a wind tunnel. The simulations demonstrated that the SKE, New-SKE, RKE, and SST models were not far off from the experimental data, while the RNG $k-\varepsilon$ model was in close agreement with it. To balance computing cost and solution accuracy for such a highly dynamic flow behavior of pollutants transport phenomena, statistical performance analysis has shown RANS technique to be still appropriate. Furthermore, a drastic change in the flow pattern was observed with varying aspect ratios and the introduction of the extended balconied structure. This indicated that a simple change in the structural configuration of the building can affect the transport of pollutants, so such kind of flow is highly sensitive to these things. Hence, accurate replication of these models can help to predict the pollution-prone location so that the pedestrians or the residents of these buildings can avoid such places. On the basis of the above numerical study, the following concluding remarks are drawn:

1. RNG $k-\varepsilon$ model proved to be the best fit among other standard RANS turbulence models mean FB -0.105, NMSE 0.045, FAC2 0.915, and R 0.93.
2. According to our findings, street canyons with a low AR of 0.2 can effectively promote the escape of pollutants with CFR 1.452 compared to the ARs of 0.5 and 1. An increase of dispersion by 51.4% for AR=0.2 and by 42.33% for AR=0.5 was observed in comparison to AR=1. Higher ARs result in flow fields that are more constrained and stagnant, which restricts the dispersion of pollutants.
3. The results show that adding balconies can lower the concentration of gaseous pollutants in some regions only. The balcony configuration LW-B, W-B, and L-B reduced the exchange concentration flux of pollutants with atmospheric air above the street canyon by 55.58%, 12.94%, and 12.1% respectively than the N-B case. An important observation was although CFR was highest for N-B; CR is still high in comparison to other balconied structures (predominantly at wall A). The LW-B, L-B, and W-B balcony configuration caused averaged concentration on wall A to reduce by 43.75 %, 13% and 4.75% whereas on wall B to increase by 24.05%, 2.75% and 80.55% respectively. This suggests that most gaseous pollutants escape from near the top face of the building. Pollution is still less in the street region, which contradicts most cases of LW-B, L-B, and W-B cases.

4. Increased wind speeds caused higher dispersion of concentration in the street canyon of Baghbazar and become diluted, resulting in lower concentrations on these buildings. Conversely, when wind speed decreases, pollutants can become trapped and accumulate in specific areas, leading to higher concentrations in buildings.

Therefore, the proposed numerical model was shown reliable and is very useful to design building configurations in smart urban cities to reduce the risk of pollution. To address the issue of pollution and improve air quality in Baghbazar, it is recommended to leave spacing between buildings to allow for better flow interaction. This can help to prevent the formation of wind vortices and eddies that can trap and accumulate pollutants in specific areas, leading to higher concentrations in buildings. Along with this, the addition of a balcony in the building showed different variations in flow patterns. Hence, such structures can be added or removed from the buildings to achieve the best dispersion of pollutants at the desired location because flow patterns are very sensitive to these configurations.

6.2. Recommendations

The following are the recommendations made by the authors:

- Unsteady calculations are expected to generate more accurate predictions since these kinds of flow are highly transient in nature.
- The concentration flow rate at the source for Baghbazar's case is arbitrary which can be an important parameter to consider. Pollutants from the ambient environment along with averaged-out concentration data from the street over time could be used.
- Design optimization such as roof shape of the buildings, chimney structures, wind catcher, vegetation like trees, etc can be modeled to enhance the pollutant dispersion in street canyon.

References

- [1] F Albrecht. Untersuchungen der vertikalen luftzirkulation in der grossstadt. *Met. Zt*, 50:93–98, 1933.
- [2] Department of Hydrology and Meteorology Nepal. Wind speed data at tribhuvan international airport. <https://www.dhm.gov.np/>, 2022.
- [3] Department of Urban Development and Building Construction Nepal. Architectural design requirements. <http://www.dudbc.gov.np/buildingcode>, 2015.
- [4] World Health Organization. Air pollution. https://www.who.int/health-topics/air-pollution#tab=tab_1, 2022.
- [5] IQAIR. Air quality in kathmandu. <https://www.iqair.com/nepal/central-region/kathmandu>, 2022.
- [6] World Population Review. Kathmandu population. <https://worldpopulationreview.com/world-cities/kathmandu-population>, 2023.
- [7] Department of Transport Management. Total number of registered motor vehicles in nepal. <https://www.dotm.gov.np/>, 2022.
- [8] Kabindra M Shakya, Maheswar Rupakheti, Anima Shahi, Rejina Maskey, Bidya Pradhan, Arnico Panday, Siva P Puppala, Mark Lawrence, and Richard E Peltier. Near-road sampling of pm 2. 5, bc, and fine-particle chemical components in kathmandu valley, nepal. *Atmospheric Chemistry and Physics*, 17(10):6503–6516, 2017.
- [9] Enna Mool, Prakash V Bhawe, Nita Khanal, Rejina M Byanju, Sagar Adhikari, Bhupendra Das, Siva P Puppala, et al. Traffic condition and emission factor from diesel vehicles within the kathmandu valley. *Aerosol and Air Quality Research*, 20(3):395–409, 2020.
- [10] Tim R Oke. Street design and urban canopy layer climate. *Energy and buildings*, 11(1-3):103–113, 1988.
- [11] Michael Schatzmann, Helge Olesen, and Jörg Franke. *COST 732 model evaluation case studies: approach and results*. 01 2010.
- [12] HW Georgii, HW Busch, and E Weber. Investigation of the temporal and spatial distribution of the emission concentration of carbon monoxide in frankfurt. *Frankfurt, Germany: Report*, (11of):102–140, 1967.

- [13] A Walton and AYS Cheng. Large-eddy simulation of pollution dispersion in an urban street canyon—part ii: idealised canyon simulation. *Atmospheric Environment*, 36(22):3615–3627, 2002.
- [14] A Walton and AYS Cheng. Large-eddy simulation of pollution dispersion in an urban street canyon—part ii: idealised canyon simulation. *Atmospheric Environment*, 36(22):3615–3627, 2002.
- [15] Michel Pavageau and Michael Schatzmann. Wind tunnel measurements of concentration fluctuations in an urban street canyon. *Atmospheric environment*, 33(24-25):3961–3971, 1999.
- [16] Jong-Jin Baik and Jae-Jin Kim. A numerical study of flow and pollutant dispersion characteristics in urban street canyons. *Journal of applied meteorology*, 38(11):1576–1589, 1999.
- [17] Xian-Xiang Li, Chun-Ho Liu, and Dennis YC Leung. Development of $k-\epsilon$ model for the determination of air exchange rates for street canyons. *Atmospheric environment*, 39(38):7285–7296, 2005.
- [18] Keer Zhang, Guanwen Chen, Xuemei Wang, Shanhe Liu, Cheuk Ming Mak, Yifan Fan, and Jian Hang. Numerical evaluations of urban design technique to reduce vehicular personal intake fraction in deep street canyons. *Science of the Total Environment*, 653:968–994, 2019.
- [19] Keer Zhang, Guanwen Chen, Yong Zhang, Shanhe Liu, Xuemei Wang, Baoming Wang, and Jian Hang. Integrated impacts of turbulent mixing and $\text{NO}_x\text{-O}_3$ photochemistry on reactive pollutant dispersion and intake fraction in shallow and deep street canyons. *Science of the Total Environment*, 712:135553, 2020.
- [20] Lup Wai Chew, Amir A Aliabadi, and Leslie K Norford. Flows across high aspect ratio street canyons: Reynolds number independence revisited. *Environmental Fluid Mechanics*, 18:1275–1291, 2018.
- [21] Hee Chang Lim, Ian P Castro, and Roger P Hoxey. Bluff bodies in deep turbulent boundary layers: Reynolds-number issues. *Journal of Fluid Mechanics*, 571:97–118, 2007.
- [22] AAR Townsend. *The structure of turbulent shear flow*. Cambridge university press, 1980.
- [23] Lionel Soulhac, P Mejean, and RJ Perkins. Modelling the transport and dispersion of pollutants in street canyons. *International journal of environment and pollution*, 16(1-6):404–413, 2001.

- [24] John M Crowther and Abdel Galeil AA Hassan. Three-dimensional numerical simulation of air pollutant dispersion in street canyons. *Water, Air and Soil Pollution: Focus*, 2(5):279–295, 2002.
- [25] Jong-Jin Baik and Jae-Jin Kim. On the escape of pollutants from urban street canyons. *Atmospheric Environment*, 36(3):527–536, 2002.
- [26] Hong Huang, Yoshiaki Akutsu, Mitsuru Arai, and Masamitsu Tamura. A two-dimensional air quality model in an urban street canyon: evaluation and sensitivity analysis. *Atmospheric Environment*, 34(5):689–698, 2000.
- [27] Xing Zheng, Hamid Montazeri, and Bert Blocken. Impact of building façade geometrical details on pollutant dispersion in street canyons. *Building and Environment*, 212:108746, 2022.
- [28] F Murena and B Mele. Effect of balconies on air quality in deep street canyons. *Atmospheric Pollution Research*, 7(6):1004–1012, 2016.
- [29] Yuhan Huang, Chengwang Lei, Chun-Ho Liu, Pascal Perez, Hugh Forehead, Shaofei Kong, and John L. Zhou. A review of strategies for mitigating roadside air pollution in urban street canyons. *Environmental Pollution*, 280:116971, 2021.
- [30] Nicolas Reiminger, José Vazquez, Nadège Blond, Matthieu Dufresne, and Jonathan Wertel. Cfd evaluation of mean pollutant concentration variations in step-down street canyons. *Journal of Wind Engineering and Industrial Aerodynamics*, 196:104032, 2020.
- [31] Soo-Jin Park, Jae-Jin Kim, Wonsik Choi, Eun-Ryoung Kim, Chang-Keun Song, and Eric R Paradyjak. Flow characteristics around step-up street canyons with various building aspect ratios. *Boundary-Layer Meteorology*, 174:411–431, 2020.
- [32] Wei Tan, Chaojie Li, Kang Wang, Guorui Zhu, and Liyan Liu. Geometric effect of buildings on the dispersion of carbon dioxide cloud in idealized urban street canyons. *Process Safety and Environmental Protection*, 122:271–280, 2019.
- [33] Cheng-Hsin Chang and Robert Meroney. Numerical and physical modeling of bluff body flow and dispersion in urban street canyons. *Journal of Wind Engineering and Industrial Aerodynamics*, 89:1325–1334, 12 2001.
- [34] Zahra Jandaghian. Flow and pollutant dispersion model in a 2d urban street canyons using computational fluid dynamics. *Computational Engineering and Physical Modeling*, 1(1):83–93, 2018.

- [35] Hesheng Yu and Jesse Thé. Simulation of gaseous pollutant dispersion around an isolated building using the $k-\omega$ sst (shear stress transport) turbulence model. *Journal of the Air & Waste Management Association*, 67(5):517–536, 2017. PMID: 27650217.
- [36] Bayesian calibration of the constants of the $k-\epsilon$ turbulence model for a cfd model of street canyon flow. *Computer Methods in Applied Mechanics and Engineering*, 279:536–553, 2014.
- [37] B. Blocken, Ted Stathopoulos, P. Saathoff, and X. Wang. Numerical evaluation of pollutant dispersion in the built environment: Comparisons between models and experiments. *Journal of Wind Engineering and Industrial Aerodynamics*, 96:1817–1831, 10 2008.
- [38] Bert Blocken. Computational fluid dynamics for urban physics: Importance, scales, possibilities, limitations and ten tips and tricks towards accurate and reliable simulations. *Building and Environment*, 91:219–245, 2015.
- [39] Robert N Meroney, Stillianos Rafailidis, and Michel Pavageau. Dispersion in idealized urban street canyons. In *Air Pollution Modeling and Its Application XI*, pages 451–458. Springer, 1996.
- [40] Anton Petrov. Evaluation of openfoam against codasc wind tunnel data base and impact of heating on the flow in an idealized street canyon, 10 2017.
- [41] Laboratory of Building and Environmental Aerodynamics. Codasc. <https://www.umweltaerodynamik.de/bilder-originale/CODA/CODASC.html>, 2008.
- [42] Department of Environment Nepal. Status of air quality in nepal annual report. https://doenv.gov.np/progressfiles/Status-of-Air-Quality-in-Nepal-Annual-Report_2021-1676438644.pdf, 2023.
- [43] Cadmapper. <https://cadmapper.com/>.
- [44] Hao Zhang, Tiantian Xu, Yuzhao Zong, Huajun Tang, Xueting Liu, and Yuancheng Wang. Influence of meteorological conditions on pollutant dispersion in street canyon. *Procedia Engineering*, 121:899–905, 2015.

A. SOLVER

A.1. turbScalarTransportSimpleFoam.C

```
/*
-----*\
=====
\\      /  F i e l d      |  OpenFOAM: The Open Source CFD Toolbox
\\      /  O p e r a t i o n  |
\\      /  A n d            |  www.openfoam.com
  \\\   /  M a n i p u l a t i o n  |
-----*\

    Copyright (C) 2011–2017 OpenFOAM Foundation
-----*\

License
    This file is part of OpenFOAM.

Application
    turbScalarTransportSimpleFoam

Description
    This is a combination of two solvers i.e. scalarTransportFoam and
    simpleFoam for the turbulent transport
    of the scalars. The code developed is used for a passive transport of
    the pollutants such as CO, COx, NOx,
    etc . Hence, the solver aims to model the pollutant dispersion
    phenomenon using CFD techniques in
    opensource software OpenFOAM.

-----*\
*/

#include "fvCFD.H"
#include "singlePhaseTransportModel.H"
#include "turbulentTransportModel.H"
#include "simpleControl.H"
#include "fvOptions.H"

// * * * * *
* * //
```

```

int main(int argc , char *argv [])
{
    argList::addNote
    (
        "Steady-state solver for incompressible, turbulent flows."
    );

    #include "postProcess.H"
    #include "addCheckCaseOptions.H"
    #include "setRootCaseLists.H"
    #include "createTime.H"
    #include "createMesh.H"
    #include "createControl.H"
    #include "createFields.H"
    #include "initContinuityErrs.H"

    turbulence->validate();

    // * * * * *
    // * * //

    Info<< "\nStarting time loop\n" << endl;

    while (simple.loop())
    {
        Info<< "Time=_" << runTime.timeName() << nl << endl;

        // --- Pressure-velocity SIMPLE corrector
        {
            #include "UEqn.H"
            #include "pEqn.H"
        }

        laminarTransport.correct();
        turbulence->correct();

        #include "CEqn.H"

        runTime.write();

        runTime.printExecutionTime(Info);
    }

    Info<< "End\n" << endl;

    return 0;
}

```

```

}

//
*****
//

```

A.2. UEqn.H

```

// Momentum predictor

MRF.correctBoundaryVelocity(U);

tmp<fvVectorMatrix> tUEqn
(
    fvm::div(phi, U)
  + MRF.DDt(U)
  + turbulence->divDevReff(U)
  ==
    fvOptions(U)
);
fvVectorMatrix& UEqn = tUEqn.ref();

UEqn.relax();

fvOptions.constrain(UEqn);

if (simple.momentumPredictor())
{
    solve(UEqn == -fvc::grad(p));

    fvOptions.correct(U);
}

```

A.3. pEqn.H

```

{
    volScalarField rAU(1.0/UEqn.A());
    volVectorField HbyA(constrainHbyA(rAU*UEqn.H(), U, p));
    surfaceScalarField phiHbyA("phiHbyA", fvc::flux(HbyA));
    MRF.makeRelative(phiHbyA);
    adjustPhi(phiHbyA, U, p);
}

```

```

tmp<volScalarField> rAtU(rAU);

if (simple.consistent())
{
    rAtU = 1.0/(1.0/rAU - UEqn.H1());
    phiHbyA +=
        fvc::interpolate(rAtU() - rAU)*fvc::snGrad(p)*mesh.magSf();
    HbyA -= (rAU - rAtU())*fvc::grad(p);
}

tUEqn.clear();

// Update the pressure BCs to ensure flux consistency
constrainPressure(p, U, phiHbyA, rAtU(), MRF);

// Non-orthogonal pressure corrector loop
while (simple.correctNonOrthogonal())
{
    fvScalarMatrix pEqn
    (
        fvm::laplacian(rAtU(), p) == fvc::div(phiHbyA)
    );

    pEqn.setReference(pRefCell, pRefValue);

    pEqn.solve();

    if (simple.finalNonOrthogonalIter())
    {
        phi = phiHbyA - pEqn.flux();
    }
}

#include "continuityErrs.H"

// Explicitly relax pressure for momentum corrector
p.relax();

// Momentum corrector
U = HbyA - rAtU()*fvc::grad(p);
U.correctBoundaryConditions();
fvOptions.correct(U);
}

```

A.4. CEqn.H

```
{
volScalarField DCC ("DCC", DC + turbulence->nut()/Sct) ;

while (simple.correctNonOrthogonal())
{
    fvScalarMatrix CEqn
    (
        fvm::ddt(C)
        + fvm::div(phi, C)
        - fvm::laplacian(DTT, C)
        ==
        fvOptions(T)
    );

    CEqn.relax();
    fvOptions.constrain(CEqn);
    CEqn.solve();
    fvOptions.correct(C);
}
```

A.5. createFields.H

```
{

Info<< "Reading field p\n" << endl;
volScalarField p
(
    IOobject
    (
        "p",
        runTime.timeName(),
        mesh,
        IOobject::MUST_READ,
        IOobject::AUTO_WRITE
    ),
    mesh
);

Info<< "Reading field C\n" << endl;
volScalarField C
(
    IOobject
```



```

(
    "C",
    runTime.timeName(),
    mesh,
    IOobject::MUST_READ,
    IOobject::AUTO_WRITE
),
mesh
);

Info<< "Reading field U\n" << endl;
volVectorField U
(
    IOobject
    (
        "U",
        runTime.timeName(),
        mesh,
        IOobject::MUST_READ,
        IOobject::AUTO_WRITE
    ),
    mesh
);

Info<< "Reading transportProperties\n" << endl;

IOdictionary transportProperties
(
    IOobject
    (
        "transportProperties",
        runTime.constant(),
        mesh,
        IOobject::MUST_READ_IF_MODIFIED,
        IOobject::NO_WRITE
    )
);

Info<< "Reading Schmidt number Sct\n" << endl;

dimensionedScalar Sct
(
    "Sct", dimless, transportProperties
);

```

```

Info << "Reading \diffusivity \DC\n" << endl;

dimensionedScalar DC
(
    "DC", dimViscosity, transportProperties
);

#include "createPhi.H"

label pRefCell = 0;
scalar pRefValue = 0.0;
setRefCell(p, simple.dict(), pRefCell, pRefValue);
mesh.setFluxRequired(p.name());

singlePhaseTransportModel laminarTransport(U, phi);

autoPtr<incompressible::turbulenceModel> turbulence
(
    incompressible::turbulenceModel::New(U, phi, laminarTransport)
);

#include "createMRF.H"
#include "createFvOptions.H"

```

B. Simulation Data

The complete simulation data with the wind tunnel results are available in this [link](#).

C. Cross-sectional contour plots of pressure and velocity

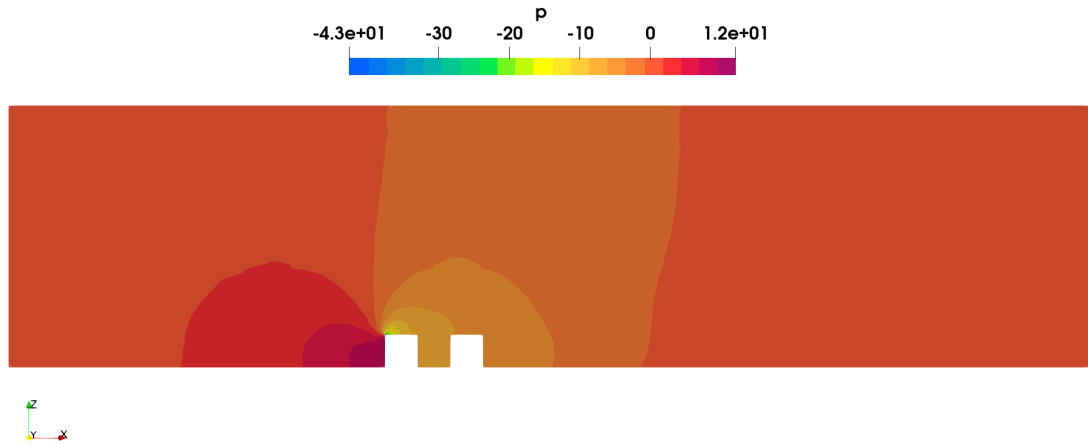


Figure C.1: Pressure field

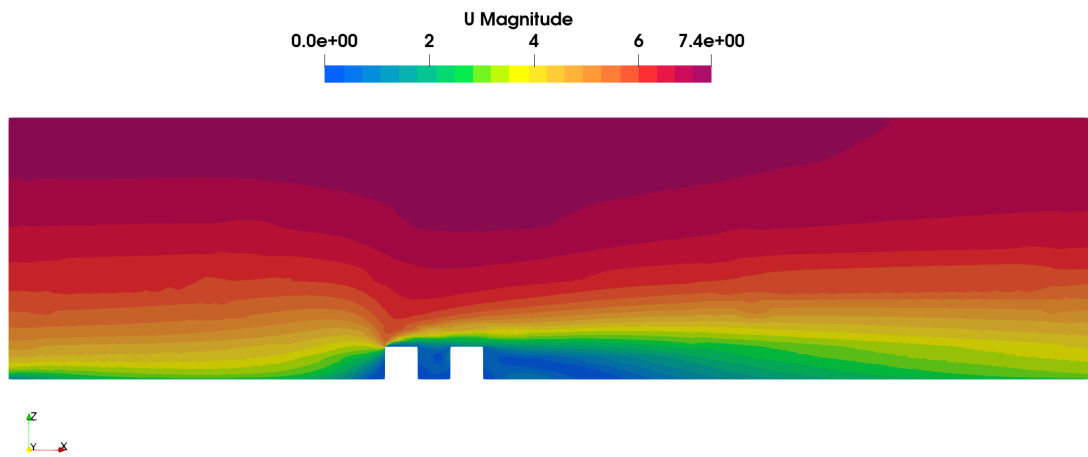


Figure C.2: Velocity field

D. Contour plots of concentration data for two design parameters

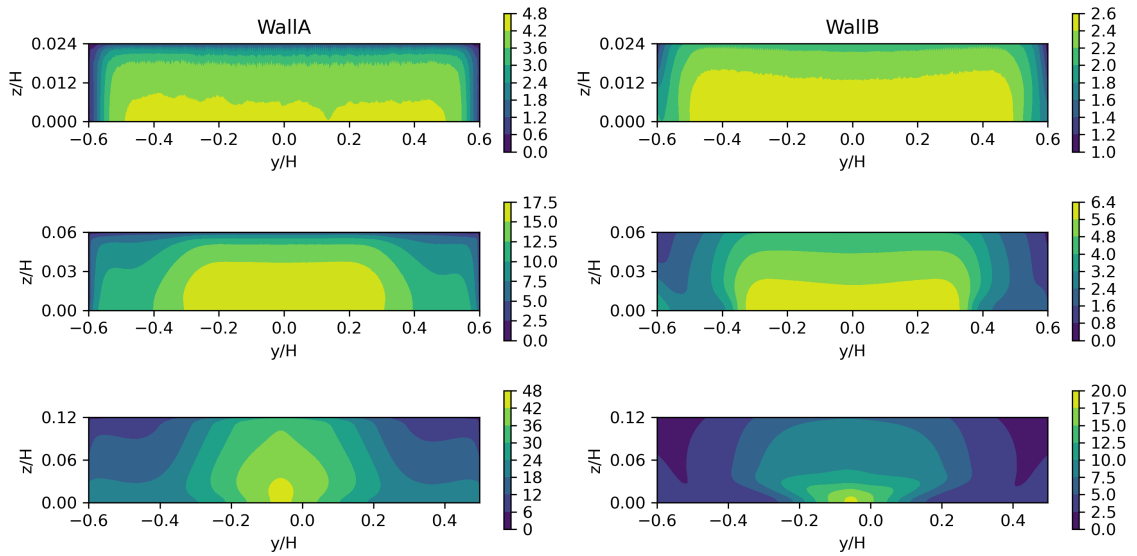


Figure D.1: Wall contours of C_p/C_s for varying aspect ratio: 0.2, 0.5 and 1

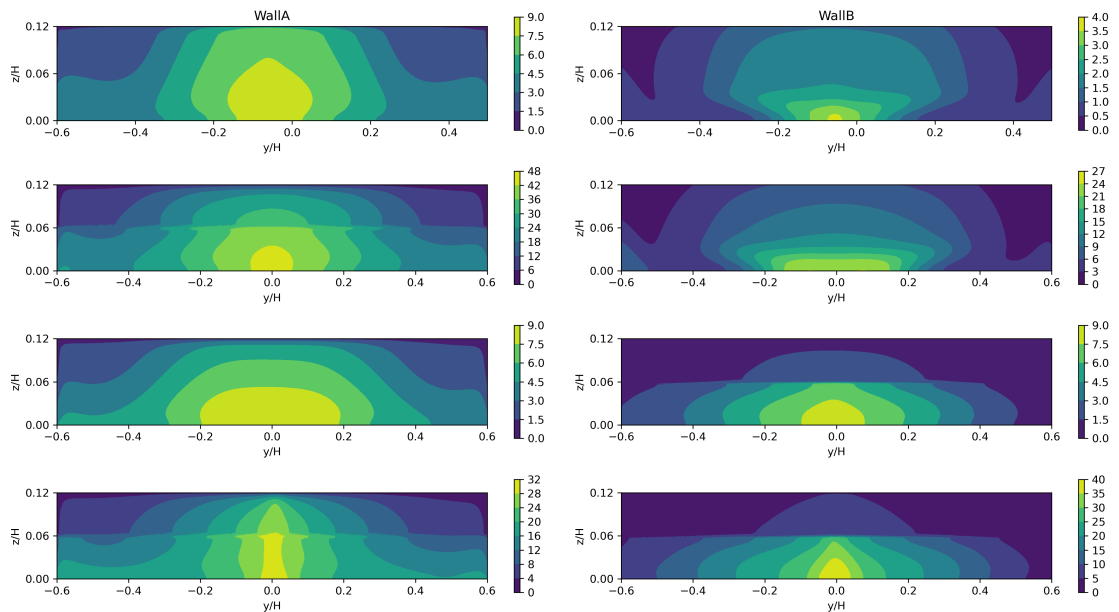


Figure D.2: Wall contours of C_p/C_s for varying balconied structure: N-B, L-B, W-B and LW-B

E. Contours of concentration at $z/H=0.5$

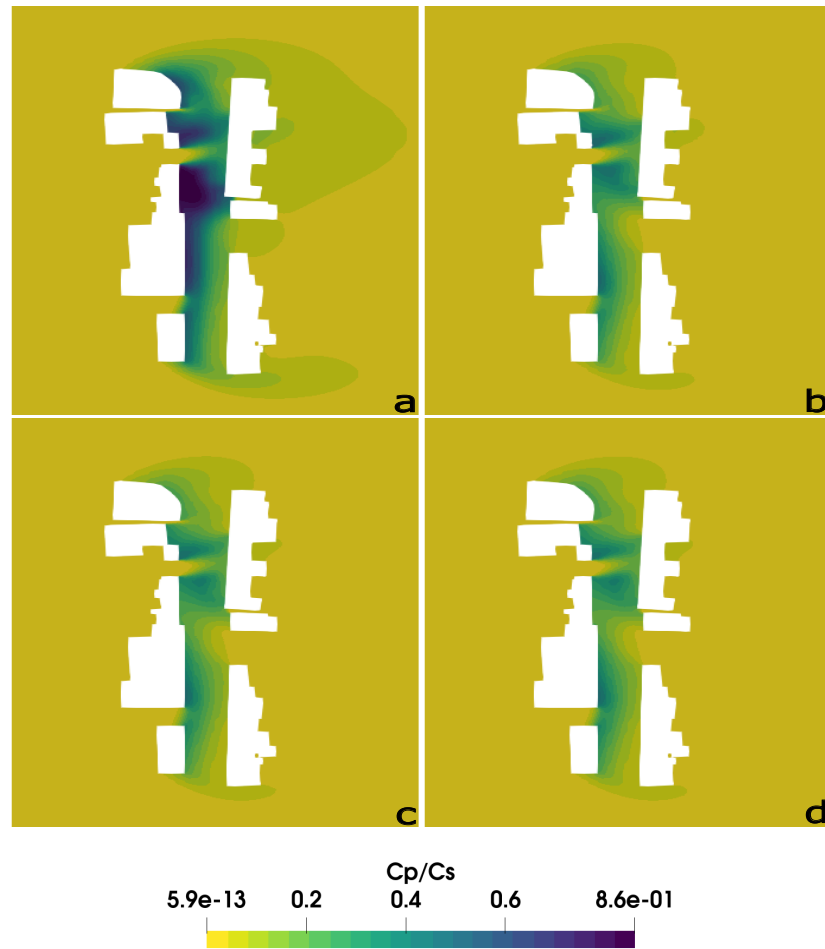


Figure E.1: Contours of C_p/C_s at $z/H=0.5$ for different u_{ref} (a) 1 knot (b) 6 knots (c) 15 knots and (d) 22 knots

F. Streamlines around Baghbazar

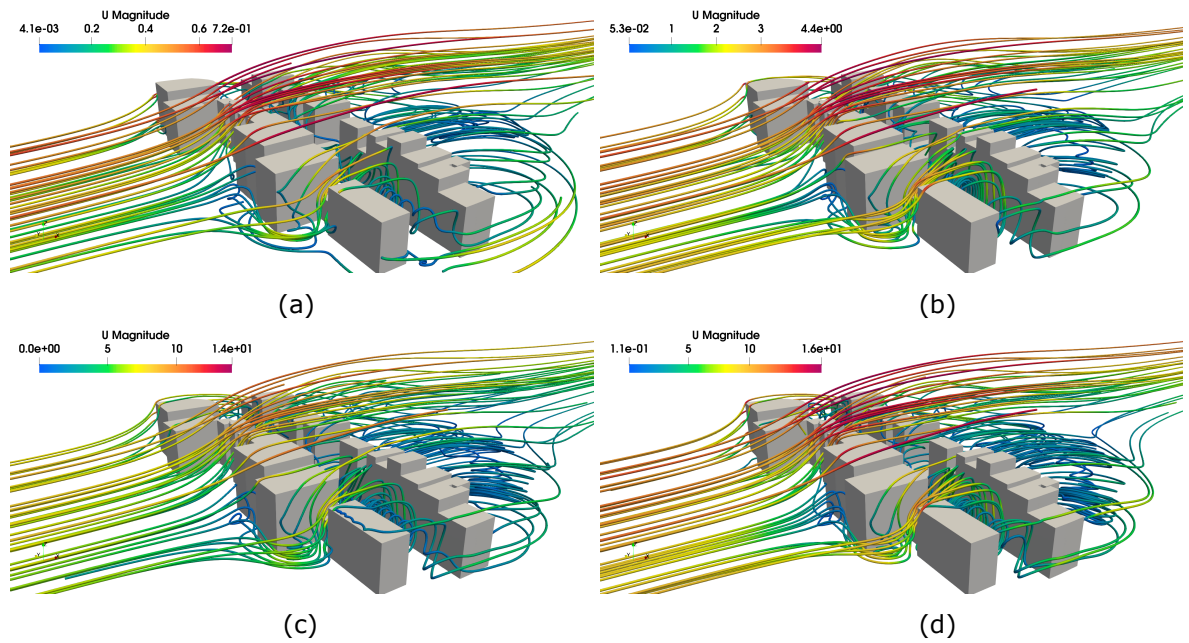


Figure F.1: Streamlines around the street canyon of Baghbazar: (a) 1 (b) 6 (c) 15 and (d) 22 knots